Lactate and glycerol-3-phosphate metabolism cooperatively regulate growth and redox balance during *Drosophila melanogaster* larval development

Hongde Li[1], Kasun Buddika[1*], Maria C. Sterrett[1*], Cole R. Julick[2], Rose C. Pletcher[1], Chelsea J. Gosney[1], Anna K. Burton[1], Jonathan A. Karty[3], Kristi L. Montooth[2], Nicholas S. Sokol[1], and Jason M. Tennessen[1§]

[1]Department of Biology, Indiana University, Bloomington, IN 47405, USA

[2]School of Biological Sciences, University of Nebraska, Lincoln, NE 68588, USA

[3] Department of Chemistry, Indiana University, Bloomington, IN, 47405, USA.

*These authors contributed equally to this work.

[§] Correspondence: jtenness@indiana.edu

Keywords: *Drosophila*, redox balance, aerobic glycolysis, lactate dehydrogenase, glycerol-3-phosphate dehydrogenase

ABSTRACT

The dramatic growth that occurs during *Drosophila* larval development requires rapid conversion of nutrients into biomass. Many larval tissues respond to these biosynthetic demands by increasing carbohydrate metabolism and lactate dehydrogenase (dLDH) activity. The resulting metabolic program is ideally suited to synthesize macromolecules and mimics the manner by which cancer cells rely on aerobic glycolysis. To explore the potential role of *Drosophila* dLDH in promoting biosynthesis, we examined how *dLdh* mutations influence larval development. Our studies unexpectantly found that *dLdh* mutants grow at a normal rate, indicating that dLDH is dispensable for larval biomass production. However, subsequent metabolomic analyses suggested that *dLdh* mutants compensate for the inability to produce lactate by generating excess glycerol-3-phosphate (G3P), the production of which also influences larval redox balance. Consistent with this possibility, larvae lacking both dLDH and G3P dehydrogenase (GPDH1) exhibit developmental delays, synthetic lethality, and aberrant carbohydrate metabolism. Considering that human cells also generate G3P upon Lactate Dehydrogenase A (LDHA) inhibition, our findings hint at a conserved mechanism in which the coordinate regulation of lactate and G3P synthesis imparts metabolic robustness upon growing animal tissues.

INTRODUCTION

Nearly a century ago, Otto Warburg observed that tumors exhibit high levels of glucose consumption coupled to oxygen-independent lactate production (Warburg, 1956). This metabolic program, which is commonly referred to as the Warburg effect or aerobic glycolysis, has become a focal point of cancer metabolism research (Vander Heiden et al., 2009). The manner by which tumors consume glucose and generate lactate, however, is not unique to either cancer cells or diseased tissue. In fact, the hallmark characteristics of aerobic glycolysis are activated under a variety of normal developmental conditions, such as during maturation of human T cells (Cooper et al., 1963; Pearce et al., 2013; Wang et al., 1976), formation of vertebrate somites (Bulusu et al., 2017; Oginuma et al., 2017), development of muscle tissue (Tixier et al., 2013), activation of hair follicle stem cells (Flores et al., 2017), and *Drosophila* larval growth (Tennessen et al., 2011). Moreover, studies of the mitochondrial pyruvate carrier (MPC1) reveal that forcibly shifting intestinal stem cells towards a more glycolytic state induces over-proliferation in both mice and flies (Bricker et al., 2012; Schell et al., 2017). Overall, these examples illustrate how the coordinate regulation of glycolytic flux and lactate metabolism play central roles in biomass production, cell fate decisions, and developmental growth (Miyazawa and Aulehla, 2018).

While the exact reason for why cells activate aerobic glycolysis *in vivo* remains debatable, one likely explanation revolves around the redox challenges imposed upon highly glycolytic cells (Vander Heiden et al., 2009). Under conditions of elevated glucose catabolism, glyceraldehyde-3-phosphate dehydrogenase (GAPDH) transfers electrons to NAD^+, resulting in the formation of NADH. These reducing equivalents must be efficiently removed from NADH because the resulting decrease in NAD^+ availability can dampen glycolytic flux and restricts growth. LDH relieves this redox burden by coupling NADH oxidation to lactate formation, thus ensuring that

63 NAD^+ is regenerated at an adequate rate. Therefore, highly glycolytic cells, whether in diseased
64 or normal tissues, become reliant on LDH to maintain redox balance. This hypothesis has long
65 been attractive to the cancer metabolism field because LDH inhibitors could hypothetically
66 interfere with tumor growth while having lesser impacts on normal tissues (Avi-Dor and Mager,
67 1956). As a result, much of our understanding regarding how LDH influences biosynthesis,
68 growth, and cell proliferation is derived from cancer cells studies.

69 The goal of using LDH inhibitors to disrupt tumor growth has a rich history rooted in the
70 observation that the pyruvate analogs, such as oxamate, inhibit the growth of HeLa cells in
71 glucose-rich media (Goldberg and Colowick, 1965; Goldberg et al., 1965). More recent analyses
72 support these early studies, demonstrating that both RNAi knockdown of *LDHA* transcripts and
73 LDHA inhibitors disrupt cell proliferation in culture and interfere with tumor growth in mouse
74 xenograft experiments (Billiard et al., 2013; Boudreau et al., 2016; Daniele et al., 2015; Fantin et
75 al., 2006; Qing et al., 2010). Moreover, a conditional *Ldha* mutation prevents the formation of
76 *KRAS*- and *EGFR*-induced non-small cell lung cancer in mice, thereby providing *in vivo* evidence
77 that some tumors require LDHA (Xie et al., 2014).

78 Despite the ability of LDHA inhibitors to disrupt the growth and tumorigenicity of certain
79 cancer cells, a growing body of evidence suggests that animal cells can compensate for the loss of
80 LDHA activity. Pancreatic cancer cell lines can become resistant to the LDHA inhibitor GNE-140
81 by increasing oxidative phosphorylation (OXPHOS) (Boudreau et al., 2016). Similarly, human
82 colon adenocarcinoma and murine melanoma cell lines that lack both LDHA and LDHB increase
83 OXPHOS and are capable of forming tumors in xenograft experiments (Zdralevic et al., 2018).
84 However, the most significant evidence that cellular metabolism readily adapts to the loss of LDH
85 activity is not based on cancer studies, but instead stems from a rare inborn error of metabolism

known as glycogen storage disease Type XI (GSD-XI), which results from loss-of-function mutations in the human *LDHA* gene (Maekawa et al., 1990). Other than reports of skin lesions and symptoms associated with exercise intolerance (Kanno et al., 1980; Yoshikuni et al., 1986), GSD-XI patients develop and grow normally (Kanno et al., 1988) which is surprising given the role of LDHA in several developmental and physiological processes. The mild symptoms experienced by GSD-XI patients not only raise the possibility that LDH inhibitors might be ineffective in a clinical setting, but also suggest that studies of animal development can identify the metabolic mechanisms that function redundantly with LDH. Toward this goal, we examined the metabolic consequences of mutating *dLdh* (FBgn0001258) in the fruit fly *Drosophila melanogaster*.

Similar to cancer cells, *Drosophila* larvae increase glycolytic metabolism and dLDH activity as a means of supporting the ~200-fold increase in body mass that occurs during this developmental stage (Graveley et al., 2011; Li et al., 2013; Rechsteiner, 1970; Tennessen et al., 2011; Tennessen et al., 2014b). To determine if this increase in dLDH activity is necessary to maintain redox balance and promote biomass accumulation, we examined how *dLdh* mutations influence larval development. We found that although *dLdh* mutants exhibit a decreased NAD^+/NADH ratio, this metabolic insult had no noticeable effect on either growth rate or biomass accumulation. Instead, metabolomic analysis revealed that *dLdh* mutants up-regulate G3P production, which also promotes NAD^+ regeneration and potentially supports larval growth despite loss of dLDH activity. We observed a similar result in *Gpdh1* (FBgn0001128) mutants, which develop normally despite a decreased NAD^+/NADH ratio. Larvae that lack both dLDH and GPDH1, however, exhibit severe growth defects, developmental delays, and synthetic lethality, thus demonstrating that these two enzymes cooperatively support larval growth. Considering that both cancer cells lines and humans GSD-XI patients also increase G3P production in response to

109 the loss of LDH-A (Billiard et al., 2013; Boudreau et al., 2016; Miyajima et al., 1995), our findings
110 suggest that fundamental aspects of this metabolic relationship are similar in both flies and
111 humans.
112

MATERIALS AND METHODS

Drosophila husbandry and genetic analysis

Fly stocks were maintained at 25ºC on Bloomington *Drosophila* Stock Center (BDSC) food. Larvae were raised and collected as previously described (Li and Tennessen, 2017). Briefly, 50 adult virgin females and 25 males were placed into a mating bottle and embryos were collected for four hours on a 35 mm molasses agar plate with a smear of yeast on the surface. Collection plates were stored inside of an empty 60 mm plastic plate and placed in a 25ºC incubator for 60 hours. All mutations and transgenes were studied in a w^{1118} background. *Gpdh1* and *dLdh* mutations were maintained in trans to the balancer chromosomes *CyO, p{GAL4-twi.G}, p{UAS-2xEGFP}* (BDSC Stock 6662) and *TM3, p{Dfd-GMR-nvYFP}, Sb*^{1} (BDSC Stock 23231), respectively. Unless noted, *dLdh* mutant larvae harbored a trans-heterozygous combination of Ldh^{16} and Ldh^{17} ($Ldh^{16/17}$) and a *dLdh* precise excision control strain ($dLdh^{prec}$) were used in all experiments (for a description of these alleles, see Li et al., 2017). *dLdh* mutant phenotypes were rescued using the previously describe transgene {*pdLdh*} (Li et al., 2017). RNAi experiments were conducted using transgenes that target either *dLdh* (BDSC stock 33640) or GFP (BDSC stock 41556).

Generation of *Gpdh1* mutations

Gpdh1 mutations were generated using a CRISPR/Cas9 approach (Gratz et al., 2013; Sebo et al., 2014). Two oligos encoding guide RNA sequences that targeted either exon 3 (5'-GGCTTCGACAAGGCCGAGGG -3') or exon 4 (5'- GATCTGATCACGACGTGTTA -3') were inserted into the BbsI site of pU6-BbSI-gRNA (Addgene). Each gRNA construct was independently injected into BDSC Stock 52669 (y^{1} *M{vas-Cas9.S}ZH-2A* w^{1118}) by Rainbow

Transgenic Flies (Camarillo, CA). The mutations $Gpdh^{A10}$ (19 bp deletion within exon 3; 5'-TCGACAAGGCCGAGGGCGG-3') and $Gpdh^{B18}$ (7 bp deletion with exon 4; 5'-ACGTGTT-3') were isolated using a PCR-based sequencing approach. All experiments described herein used a trans-heterozygous combination of these two alleles ($Gpdh^{A10/B18}$).

Generation of the *UAS-Gpdh1* transgene

The *UAS-Gpdh1* transgenic strain was generated by PCR amplifying the *Gpdh1* cDNA from *Drosophila* Genomics Resource Center (DGRC) cDNA clone FI03663 using the oligos 5'-AGAATTCATGGCGGATAAAGTAAAT-3' and 5'-AGCGGCCGCTTAAAGTTTTGGCGACGG-3'. The *Gpdh1* PCR product was inserted into the EcoRI and NotI sites of pUAST-attB (DGRC) and the resulting plasmid was injected into BDSC Stock 24867 (*M{vas-int.Dm}ZH-2A, PBac{y[+]-attP-3B}VK00031*) by Rainbow Transgenic Flies (Camarillo, CA).

Gas Chromatography-Mass Spectrometry (GC-MS) analysis

dLdh mutants and precise excision controls were analyzed using four independent targeted GC-MS-based metabolomic analyses. Samples were collected, processed and analyzed at either the University of Utah metabolomics core facility or the Indiana University Mass Spectrometry Facility as previously described (Cox et al., 2017; Li and Tennessen, 2018). Each sample contained 25 mid-L2 larvae. For all experiments, six biological replicates were analyzed per genotype. GC-MS data was normalized based on sample mass and in internal succinic-d4 acid standard. Each experiment was statistically analyzed using Metaboanalyst (metaboanalyst.ca) version 4.0 with Pareto scaling (Chong et al., 2018).

159

160 **Liquid Chromatography-Mass Spectrometry (LC-MS/MS) analysis**

161 For both *dLdh* mutants and precise excision controls, 100 mid-L2 larvae were
162 collected in a 1.5 mL microfuge tube. Each sample was immediately washed three times using ice-
163 cold PBS, all wash solution was removed, and the sample tube was drop frozen in liquid nitrogen.
164 Metabolite extraction and LC-MS analysis was performed by the University of Utah Metabolomics
165 core facility as previously described (Bricker et al., 2012; Cox et al., 2017). Data was analyzed
166 using a two-tailed student t-test.

167

168 **Colorimetric metabolite assays**

169 Glycogen, triglyceride (TAG), trehalose, and soluble protein were measured in mid-L2
170 larvae using previously described methods (Tennessen et al., 2014a). Briefly, 25 mid-L2 larvae
171 were collected from the surface of a molasses egg-laying cap that contained ~1.5 grams of yeast
172 paste and placed in a 1.5 mL microfuge tube. For each assay, at least six biological replicates were
173 collected from independent mating bottles. Samples were washed three times using ice-cold
174 phosphate buffered saline (PBS; pH 7.4). All PBS was removed from the samples and larvae were
175 homogenized in the appropriate assay buffer. 10 µL of larval homogenate was removed for
176 measuring soluble protein using a Bradford assay and the remaining homogenate was immediately
177 heat-treated at 70ºC for 5 minutes. Heat-treated samples were frozen at -80ºC until analyzed using
178 the appropriate assay.

179 NAD^+ and NADH were measured using the Amplite fluorimetric NAD^+/NADH ratio assay
180 kit (AAT Bioquest, Inc; 15263) according to instructions. Ten mid-second instar (L2) larvae were
181 washed with cold PBS and homogenized with 100 µL of the lysis buffer. The lysates were

centrifuged for 10 min at 3000 *g*, and the supernatants were collected for the analysis. Fluorescence was monitored with a Cytation 3 plate reader (BioTek) at Ex/Em=540/590 nm. The concentrations of NAD^+ and NADH were normalized to the soluble protein concentrations.

All metabolite measurements were repeated a minimum of three times with six independent samples analyzed per genotype. Data was analyzed using a two-tailed student t-test.

^{13}C-based metabolic turnover rate analysis

For measurement of metabolic turnover rates from glucose to lactate and glycerol-3-phosphate, mid-L2 larvae were fed with Semi-defined Medium (Backhaus et al., 1984) containing 25% D-glucose-$^{13}C_6$ for 2 hours, then metabolites were detected using an Agilent 6890N Gas Chromatograph with a 5973 Inert Mass Selective Detector and Gerstel MPS2 autosampler. The isotopologue distributions were corrected based on the natural abundance of elements. The metabolic turnover rate f_x was estimated based on the formula $X^L/X^T = p(1–exp(-f_x*t/X^T))$, where X^L is the amount of ^{13}C labeled metabolite (m+3), X^T is the amount of total metabolite pool, p is the percentage of glucose-$^{13}C_6$.

Graphical Representation of Metabolite Data

All figures were generated using Graphpad Prism 7.0 (version 7.0c). Metabolomic data are presented as box plots, with the box extending from the 25th to 75th percentile, the line in the middle representing the median value.

Quantification of Mitochondrial Genome Copy Number

Quantitative PCR was used to measure relative ratio of mitochondrial DNA/genomic DNA in precise excision controls and *dLdh* mutants based on a previously described strategy (Oliveira and Kaguni, 2011). Total DNA was isolated from 25 mid-L2 larvae using the Qiagen Core Gene 2 extraction kit. For mitochondrial DNA measurements, DNA samples were diluted 1:100 and the *Drosophila* mitochondrial gene *mt:CoI* was amplified using the oligos 5'-TGCTCCTGATATAGCATTCCCACGA-3' and 5'-TCCACCATGAGCAATTCCAGCGG-3'. The relative abundance of genomic DNA in the samples was measured by amplifying the *Rpl 32* genomic locus using oligos 5'-AGGCCCAAGATCGTGAAGAA-3' and 5'-TGTGCACCAGGAACTTCTTGAA-3'.

Larval Respiration Studies

We quantified routine metabolic rate in precise excision controls and *dLdh* mutants as CO_2 production using established flow-through respirometry protocols for larval *D. melanogaster* (Hoekstra and Montooth, 2013; Hoekstra et al., 2013). We measured metabolic rate for twenty biological replicates per genotype. Each biological replicate consisted of ten mid-L2 larvae that were placed in a small cap containing 0.5 mL of fly food inside of a glass respirometry chamber. The amount of CO_2 produced by the group of larvae was measured by flowing CO_2-free air through the chambers at a rate of 100 ml/min and measuring the CO_2 produced as a result of metabolism using an infrared CO_2 analyzer (Li-Cor 7000 CO_2/H_2O Analyzer; LI-COR, Lincoln, NE). Each run of the respirometer used a multiplexed system (Sable Systems International, Henderson, NV) to cycle through four chambers that contained larvae and a fifth baseline chamber that were all housed in a thermal cabinet maintained at 26°C (Tritech™ Research, Los Angeles, CA). Genotypes were randomly assigned to chambers within each run.

Within each run, two technical replicate measurements were performed for each group of larvae. Technical replicate measures were strongly correlated ($r = 0.935$). We calculated VCO_2 as the average rate of CO_2 produced across the 10 min. time interval for the first replicate measure in each run for each biological sample after correcting for any minimal drift in the baseline signal. Each group of larvae was massed using a Cubis® microbalance (Sartorius AG, Göttingen, Germany) before being placed in the respirometer. This allowed us to statistically account for the relationship between mass and metabolic rate when testing for differences between genotypes using a Type II Model regression implemented with smatR (Warton et al., 2006) in the R statistical package (Team, 2017). There was no significant difference between genotypes in the slope relating log(mass) and log(metabolic rate) (i.e., the mass-scaling exponent) ($P = 0.099$); we then tested whether genotypes differed in metabolic rate across masses (i.e., for a difference in the y intercept of the relationship between mass and metabolic rate).

Larval central nervous system (CNS) and gastrointestinal (GI) tract staining

CNS and intestine dissection and analysis were performed as previously described (Luhur et al., 2017; Luhur et al., 2014). Briefly, size- and age-synchronized larval CNSs and larval intestines were dissected in ice cold 1XPBS and fixed at room temperature for 45 minutes in 4% paraformaldehyde (Electron Microscopy Services) in 1X PBS with and without 0.3% Triton X-100, respectively. For Dpn staining, CNSs were subsequently washed with 0.3% PBT and blocked (1XPBS, 0.5% BSA) for at least 1 hour at room temperature. Primary antibody staining was performed with guinea pig anti-Dpn (provided by James Skeath, 1:500) for 5 hours at room temperature. Secondary antibody staining was performed overnight with AlexaFlour-488 conjugated goat anti-guinea pig antibodies (Life Technologies, 1:1000) and DAPI (0.5 µg/ml) at

4ºC. Larval intestines were washed with 0.1% PBT and incubated with DAPI for 15 minutes. Following these secondary washes, CNSs and intestines were mounted in Vectashield mounting medium (Vector Laboratories).

For EdU staining, dissected larval CNSs were immediately incubated in Grace's insect media supplemented with 1mM EdU. Subsequent manipulations were performed as described in the product manual (ThermoFisher C10338).

For quantifications, multiple Z-steps of individual brain lobes or posterior midguts were acquired using the Leica SP5 confocal microscope in the Light Microscopy Imaging Center at Indiana University, Bloomington. The maximum projection of each Z-stack was generated using FIJI. Dpn and EdU positive cell numbers were manually counted using Adobe Photoshop. The area of larval enterocyte nuclei was measured using FIJI.

RESULTS

dLDH maintains larval NAD^+ redox balance

To understand how lactate synthesis influences *Drosophila* larval metabolism, we used LC-MS/MS to measure the NAD^+/NADH ratio in larvae harboring a *trans-heterozygous* combination of the previously described *dLdh* loss of function alleles, $dLdh^{16}$ and $dLdh^{17}$, as well as a precise-excision control strain, $dLdh^{prec}$ (Li et al., 2017). Consistent with a model in which dLDH regulates larval redox balance, our analysis revealed that $dLdh^{16/17}$ mutant larvae exhibit a decreased NAD^+/NADH ratio (Figure 1A; Supplemental Table 1). In contrast, the ratios of NADP+/NADPH, reduced glutathione/oxidized glutathione (GSSG/GSH), and ADP/ATP were similar in both mutant and control larvae (Figure 1A; Supplemental Table 1). The abundance of AMP relative to ATP, however, was slightly elevated in *dLdh* mutants (Figure 1B; Supplemental Table 1). Overall, our results demonstrate that loss of dLDH activity interferes with the NAD^+/NADH balance of larvae raised under standard culture conditions but has minimal effects on other aspects of redox metabolism and energy production.

Despite the fact that redox balance is significantly altered in *Ldh* mutants, the phenotypic consequences of this metabolic disruption are mild. We previously demonstrated that *dLdh* mutant larvae raised under ideal culture conditions can grow at a normal rate for much of larval development (Li et al., 2017). Furthermore, *dLdh* mutants that survive the mid-L3 lethal phase develop into adults (Li et al., 2017). To determine if any other biosynthetic processes are disrupted in *dLdh* mutants, we quantified the major larval pools of stored energy. Our analysis revealed that loss of dLDH activity has no effect on either triglyceride or trehalose levels (Figure 1C). Meanwhile, glycogen levels exhibited a modest, but significant increase in *dLdh* mutants when compared with control larvae (Figure 1C). This later observation was notable because the

285 epidermis of human GSD-XI patients also appear to accumulate excess glycogen (Yoshikuni et
286 al., 1986), indicating that *dLdh* mutants phenocopy the subtle metabolic defects observed in
287 humans lacking LDHA.
288
289 **G3P levels are elevated in *dLdh* mutants**
290 The ability of *dLdh* mutants grow at a normal rate suggests that *Drosophila* development
291 adapts to the loss of dLDH activity. In this regard, human cell culture studies suggest that LDH-A
292 inhibition can increase flux from glycolysis into the tricarboxylic acid cycle (TCA cycle) (Billiard
293 et al., 2013; Xie et al., 2014). We found no evidence, however, that this metabolic shift occurs in
294 flies, as *dLdh* mutant and control larvae produced CO_2 at similar rates (Figure 1D). Furthermore,
295 mitochondrial DNA content was unchanged in *Ldh* mutants (Supplemental Figure 1A), suggesting
296 that loss of dLDH activity does not induce excess mitochondrial proliferation. Since our initial
297 metabolic characterization failed to provide an adequate explanation for how larvae compensate
298 for the loss of LDH, we turned to an untargeted metabolomics approach to poll a larger pool of
299 analytes. Four independent GC-MS-based studies revealed that $dLdh^{16/17}$ mutants exhibit
300 reproducible changes in only four metabolites: lactate, pyruvate, 2-hydroxyglutarate (2HG), and
301 G3P (Figure 2A-B, Supplemental Tables 2-6). Since previous studies have already examined the
302 relationship between dLDH and the metabolites lactate, pyruvate, and 2HG levels (Li et al., 2017),
303 we focused our efforts on understanding why the G3P pool size was increased in *dLdh* mutants.
304 To confirm that *dLdh* mutants accumulate excess G3P as the result of decreased dLDH activity,
305 we demonstrated that expression of an *dLdh* transgene (*p{dLdh}*) in *dLdh* mutant larvae can restore
306 G3P levels to those observed in $dLdh^{prec}$ control larvae (Figure 2C). Similarly, ubiquitous
307 expression of a *UAS-dLdh-RNAi* (*dLdhi*) transgene induced elevated G3P levels (Figure 2D), thus

confirming that *Drosophila* larvae accumulate excess G3P in response to the loss of dLDH activity. Considering that G3P levels are elevated in both GSD-XI patients and pancreatic cancer cells exposed to an LDH inhibitor ((Billiard et al., 2013; Boudreau et al., 2016; Miyajima et al., 1995)), our findings suggest that both flies and humans accumulate G3P to compensate for the loss of LDH activity.

GPDH1 regulates larval NAD$^+$/NADH redox balance

Since GPDH1 couples G3P synthesis to NADH oxidation, increased G3P production could provide *dLdh* mutants with an alternative means of regenerating NAD$^+$ (Figure 3A). Moreover, GPDH1 is a highly abundant protein in *Drosophila* larvae and could itself represent a key regulator of larval redox balance. To test these possibilities, we generated two *Gpdh1* loss-of-function alleles, $Gpdh1^{A10}$ and $Gpdh1^{B18}$, both of which represent frameshift mutations that either delete or truncate the C-terminal catalytic domain, which is required for GPDH1 enzyme activity (Supplemental Figure 2A-B). Larvae that harbor a *trans*-heterozygous combination of these alleles, $Gpdh1^{A10/B18}$, exhibited significantly lower G3P levels compared to controls (Figure 3B). Furthermore, ubiquitous expression of a *UAS-Gpdh1* transgene restored normal G3P levels in mutant larvae (Figure 3B), confirming that the loss of zygotic GPDH1 reduces G3P synthesis.

To determine if G3P production influences larval redox balance, we measured both NAD$^+$ and NADH levels in *Gpdh1* mutants. Similar to *dLdh* mutants, we observed that the NAD$^+$/NADH ratio in mid-L2 larvae was significantly lower in *Gpdh1* mutants as compared with a $Gpdh1^{A10/+}$ heterozygous control (Figure 3C). We also examined the extent to which GPDH1 influences NAD$^+$ levels by feeding D-glucose-$^{13}C_6$ to mid-L2 larvae and measuring the rate of lactate and G3P synthesis. Since both dLDH and GPDH1 must oxidize one molecule of NADH in order to form

one molecule of either lactate or G3P respectively (Figure 3A), we can indirectly infer the rate at which each enzyme regenerates NAD^+ based on synthesis of these metabolites. Our analysis revealed that mid-L2 larvae synthesize m+3 lactate and m+3 G3P at similar rates (Figure 3D), indicating that GPDH1 and dLDH regenerate roughly equivalent amounts of NAD^+ during larval development.

Our observation that *Gpdh1* mutants exhibit a decreased NAD^+/NADH ratio balance also implicates this enzyme in coordinating redox balance with larval energy production. G3P synthesized in the cytoplasm can be oxidized on the inner mitochondrial membrane by the FAD dependent enzyme Glycerophosphate oxidase 1 (Gpo-1; FBgn0022160) to generate ATP via oxidative phosphorylation (O'Brien and MacIntyre, 1972). Therefore, any decrease in G3P synthesis could also reduce ATP production. Consistent with this function, ATP levels were significantly decreased in *Gpdh1* mutants when compared with controls (Figure 3E). Yet, despite the role for GPDH1 in these critical metabolic processes, animals lacking zygotic GPDH1 activity exhibit only mild developmental defects. In agreement with previous reports (Bewley and Lucchesi, 1977), we found that *Gpdh1* mutants are viable through larval development and are ~15% smaller at the L2-L3 molt (Figure 3F and Supplemental Figure 2C), a result which again demonstrates how larval development is robust and can compensate for significant metabolic insults.

Gpdh1; dLdh double mutants exhibit severe developmental delays and a synthetic lethal phenotype

Since dLDH and GPDH1 individually control larval redox balance, we tested the possibility that simultaneous removal of both enzymes would induce growth defects. Indeed, when

compared with *Gpdh1* and *dLdh* single mutants, *Gpdh1; dLdh* double mutants are 85% smaller and experience developmental delays (Figure 4A-C). Moreover, *Gpdh1; dLdh* double mutants die throughout L1 and L2 development, with ~30% of double mutant larvae dying during L1 development and all animals failing to complete the L2-L3 molt (n>100; Figure 4C). To further characterize these growth defects in double mutant larvae, we examined the larval brain, which was previously reported to display high levels of both dLDH and GPDH1 activity (Rechsteiner, 1970). w^{1118} controls, *Gpdh1* and *dLdh* single mutants, and *Gpdh1; dLdh* double mutants were collected 60 hours after egg-laying and the brains were fixed and stained with DAPI, to visualize overall tissue size, and for Deadpan (Dpn), to visualize neuroblasts (Figure 4D-H). While the brains of single mutant larvae exhibited no growth defects, the brains of *Gpdh1; dLdh* double mutants were significantly smaller than controls (Figure 4D-G). However, if *Gpdh1; dLdh* double mutants were allowed to develop for an additional 24 hours, the brain grew to a comparable size as the w^{1118} control (Figure 4D,H). We observed a similar phenomenon in the larval intestine, where the posterior midgut of age-matched *Gpdh1; dLdh* mutant larvae was shorter than either single mutant, contained significantly smaller enterocyte nuclei, and exhibited a growth delay of approximately 24 hours when compared with single mutant controls (Supplemental Figure 3). To determine if these growth phenotypes are associated with a decreased rate of cell cycle progression, we dissected brains from size-matched larvae and incubated them in an organ culture media with EdU for 2 hours. When compared with w^{1118} controls, *dLdh* single mutants, and *Gpdh1* single mutants, the number of cells that stain with EdU was significantly decreased in *Gpdh1; dLdh* mutant brains (Figure 5A-E). Overall, these results demonstrate that while larval development can compensate for the loss of either dLDH or GPDH1, removal of both enzymes severely restricts tissue growth.

Simultaneous loss of dLDH and GPDH1 induces defects in carbohydrate and amino acid metabolism

Since our metabolic studies suggested that dLDH and GPDH1 maintain the larval NAD^+/NADH ratio, we next examined the possibility that the *Gpdh1; dLdh* double mutant growth phenotypes stem from a severe disruption of redox balance. These experiments revealed, however, that the ratio of NAD^+ to NADH was similar in control and double mutant larvae (Figure 6A). To further investigate this unexpected result, we used a targeted GC-MS-based approach to analyze central carbon metabolism of both *Gpdh1* single mutants and *Gpdh1; dLdh* double mutants (Figure 6B-D; Supplemental Tables 7 and 8). In the case of the *Gpdh1* mutant larvae, metabolomic analysis revealed a significant disruption of amino acid metabolism. Not only were aspartate and several essential amino acids decreased, but we also observed elevated levels of urea and the urea cycle intermediate ornithine (Figure 5B-D), suggesting that loss of GPDH1 results in elevated amino acid catabolism. Moreover, our analysis also uncovered elevated glutamate and proline levels. Considering that insects can synthesize proline in a NADH dependent manner (Mccabe and Bursell, 1975), this finding hints at a mechanism by which loss of G3P production induces elevated proline synthesis in response to aberrant redox balance. Intriguingly, *Gpdh1* mutants do not exhibit an increase in either lactate or 2HG levels (Figure 6B,C) – a result which would support the inverse correlation between GPDH1 and dLDH activity. This null result, however, could indicate that dLDH activity is saturated in developing larvae. Finally, xanthine and urate levels, which are produced by purine catabolism, were also increased in *Gpdh1* mutants (Figure 6B; Supplemental Figure 4A).

399 Nearly all of the metabolic changes observed in the *Gpdh1* single mutant were enhanced
400 in the *Gpdh1; dLdh* double mutants (Figure 6B,D). For example, *Gpdh1; dLdh* mutant larvae
401 exhibited a 500-fold increase in xanthine levels when compare to the heterozygous controls (Figure
402 6B; Supplemental Figure 4B), suggesting a severe disruption of purine metabolism. Overall, the
403 metabolic changes observed in the double mutant represented the combined metabolic disruptions
404 seen in the single mutants (Figure 6B-D), but with two major exceptions – the relative abundance
405 of both trehalose and glucose were significantly elevated in *Gpdh1; dLdh* mutant larvae (Figure
406 6B,D). This result is important as it suggests that the loss of both enzymes lead to decreased
407 glycolytic flux. Since an inhibition of glucose catabolism would result in decreased NADH
408 formation, the *Gpdh1; dLdh* mutant metabolomic profile provides an explanation for why the
409 NAD^+/NADH ratio is normal in double mutants. Moreover, we also observed that ATP levels are
410 dramatically decreased in $Gpdh^{A10/B18}$; $dLdh^{16/17}$ double mutants when compared with $Gpdh^{A10/+}$;
411 $dLdh^{16/+}$ heterozygous controls (Supplemental Figure 4C). This result demonstrates that loss of
412 both enzymes limits ATP production and is consistent with a model in which glycolytic flux is
413 restricted in double mutant larvae. Overall, our metabolomic approach not only demonstrates that
414 the growth defects caused by loss of both dLDH and GPDH1 are associated with severe disruption
415 of central carbon metabolism but also highlights the plasticity of animal metabolism.
416

DISCUSSION

Our findings demonstrate that the ability of dLDH and GPDH1 to cooperatively regulate NAD^+/NADH redox balance and carbohydrate metabolism imparts robustness on larval growth. This relationship likely serves multiple purposes, as the production of lactate and G3P metabolism not only influences larval NAD^+/NADH redox balance, but also controls the pool size of glycolytic intermediates and dictates the manner by which cells generate ATP. Considering that human cells also up-regulate GPDH1 activity in response to decreased lactate synthesis, our findings indicate that this metabolic relationship is conserved across animal phyla and hint at a mechanism by which GPDH1 activity could render tumors resistant to LDH inhibitors.

The roles of LDH and GPDH1 in cancer and animal development

The possibility of using LDH inhibitors to disrupt tumor growth was first proposed over 60 years ago, shortly after the discovery that the pyruvate analog oxamate disrupts aerobic glycolysis and slows the growth of HeLa cells (Goldberg and Colowick, 1965; Papaconstantinou and Colowick, 1961). During the last decade, the goal of using LDH inhibitors as chemotherapeutic agents has been revisited, with several studies demonstrating that this approach can disrupt cancer cell growth (Billiard et al., 2013; Boudreau et al., 2016; Daniele et al., 2015; Fantin et al., 2006; Qing et al., 2010). Yet, despite the promise of such compounds, studies of human and mouse *LDHA* mutants raise concerns about the potential effectiveness of inhibiting LDH. First, GSD-XI patients grow and develop normally (Kanno et al., 1988; Kanno et al., 1980; Miyajima et al., 1995), suggesting that human developmental metabolism can compensate for loss of this enzyme. Secondly, although *LDHA* inhibition induces elevated TCA cycle flux in cell culture, this reliance on the TCA cycle is not observed in neither tumors derived from conditional

441 *LDHA* mutant nor *ex vivo* tumor slices treated with an LDH inhibitor (Xie et al., 2014). Such
442 observations are important because they suggest that the metabolic plasticity of cells in culture
443 differs significantly from tissues *in vivo*.

444 Our studies in the fly support the *in vivo* mammalian observations – *dLdh* mutants grow
445 normally and do not increase CO_2 production, indicating that flux through the TCA cycle is
446 unchanged. Instead, we observed that *dLdh* mutants specifically up-regulate G3P synthesis as a
447 means of maintaining developmental growth. This finding is consistent with decades of
448 observation in tumors, insects, and healthy human tissues, which, on the whole, repeatedly pointed
449 to an inverse correlation between lactate and G3P production (Boxer and Shonk, 1960; Miyajima
450 et al., 1995; Rechsteiner, 1970; Zebe and McShan, 1957). Moreover, recent cell culture studies
451 have also demonstrated that LDH inhibitors induce G3P synthesis, thus demonstrating that this
452 metabolic relationship is present in cultured cells (see supplemental data in Billiard et al., 2013;
453 Boudreau et al., 2016). Overall, our observations in the fly suggest a common metabolic
454 relationship that allows animal cells to adapt to redox stress.

455 The link between larval redox balance and the role of G3P in ATP production could also
456 explain a contradiction in the *Drosophila* metabolism literature. Mutations that disrupt either
457 glycolysis (*e.g. dERR, Pfk*) or the electron transport chain (ETC) result in severe growth defects
458 (Mandal et al., 2005; Meiklejohn et al., 2013; Tennessen et al., 2011). In contrast, larvae that harbor
459 mutations in either the *mitochondrial pyruvate carrier* (*dMPC1*) or *malate dehydrogenase 2* are
460 able to complete larval development with relatively mild phenotypes (Bricker et al., 2012; Wang
461 et al., 2010). Similarly, larvae that lack zygotic *isocitrate dehydrogenase 3b* exhibit developmental
462 delays but are able to survive until metamorphosis (Duncan et al., 2017). These observations
463 suggest that while glycolysis and oxidative phosphorylation are necessary for development, larvae

464 do not require a fully functional TCA cycle. This arrangement makes sense in that larval
465 metabolism is largely dedicated to shuttling metabolic intermediates into biosynthetic pathways.
466 By activating GPDH1, the production of G3P helps regenerate cytosolic NAD^+ without increasing
467 CO_2 production while also allowing cells to transfer reducing equivalents to the ETC and generate
468 ATP.
469
470 **_Drosophila_ as a model for studying metabolic plasticity**
471 Our study highlights the remarkable metabolic plasticity that underlies animal development
472 and physiology. Intermediary metabolism adapts to a surprisingly broad range of natural genetic
473 variation, dietary stress, and metabolic insults. For example, mutations in the *Drosophila*
474 mitochondrial pyruvate carrier *dMPC1*, which render cells unable to transport pyruvate into the
475 mitochondria, elicit no obvious phenotypes when mutant larvae are raised under standard growth
476 conditions (Bricker et al., 2012). Moreover, natural populations of *Drosophila* can buffer larval
477 development against significant variations in mitochondrial oxidative capacity and the scaling
478 relationship between mass and metabolic rate (Matoo et al., 2018). A similar phenomenon is also
479 observed in *C. elegans*, where entire metabolic pathways are rewired in response to dietary stress
480 or genetic mutations (MacNeil et al., 2013; Watson et al., 2014; Watson et al., 2016). These
481 examples not only highlight the adaptability of animal metabolism, but also emphasize how little
482 we understand about this topic. The molecular mechanisms that control adaptive metabolic
483 rewiring, however, are often difficult to study in a laboratory setting, where animals are raised on
484 high nutrient diets and buffered against the environmental stress. In this regard, recent advances
485 in metabolomics provides a powerful approach for understanding how metabolism adapts to
486 environmental and genetic insults. By analyzing changes in gene expression within the context of

487 metabolomic data, compensatory changes in metabolic flux can be quickly identified and analyzed
488 using standard model organism genetics. The power of this approach is demonstrated by our
489 studies of *dLdh*. Even without prior knowledge of the link between LDH and GPDH1 activity, our
490 study pinpointed increased G3P synthesis as the adaptive response within *dLdh* mutants, thus
491 demonstrating how metabolomics holds the potential to illuminate the complex metabolic network
492 that supports animal development.
493

494 **ACKNOWLEDGEMENTS**

495 We thank the Bloomington *Drosophila* Stock Center (NIH P40OD018537) for providing fly
496 stocks, the *Drosophila* Genomics Resource Center (NIH 2P40OD010949) for genomic reagents,
497 and Flybase (NIH 5U41HG000739). Targeted GC-MS analysis was conducted using instruments
498 housed in the Indiana University Mass Spectrometry Facility, which is supported, in part, by NSF
499 MRI Award 1726633. Some of the metabolomic analyses described herein performed at the
500 Metabolomics Core Facility at the University of Utah, which is supported by 1S10OD016232-01,
501 1S10OD021505-01 and 1U54DK110858-01. Special thanks to Madhulika Rai for useful
502 comments. C.J.G. was supported, in part, by the Lawrence University LU-R1 program. K.B. and
503 N.S.S. were supported by National Institute of Health Award R01GM124220. C.R.J. was
504 supported by NSF CAREER award to K.L.M. (IOS-1149178, IOS-1505247). J.M.T. is supported
505 by the National Institute of General Medical Sciences of the National Institutes of Health under a
506 R35 Maximizing Investigators' Research Award (MIRA; 1R35GM119557).
507

FIGURE LEGENDS

Figure 1. dLDH maintains the NAD^+/NADH redox balance during larval development. Targeted LC-MS/MS analysis was used to measure metabolites associated with redox balance in *dLdh^{prec}* controls and *dLdh$^{16/17}$* mutants. The ratio of (A-B) NAD^+/NADH, $NADP^+$/NADPH, GSH/GSSG, AMP/ATP and ADP/ATP were determined in control and mutant larvae. n=8 samples collected from independent populations with 100 mid-L2 larvae per sample. (C) *dLdh^{prec}* controls and *dLdh$^{16/17}$* mutants were collected as mid-L2 larvae and the concentration of triglycerides (TAG), trehalose (Treh), and glycogen (Glyc) were measured in whole animal homogenates. All data were normalized to soluble protein. For all assays, n>10 samples collected from independent populations with 25 mid-L2 larvae per sample. (D) The rate of CO_2 production was measured *dLdh$^{16/17}$* mutants and precise excision controls. For (A-C), * $P < 0.05$. *** $P < 0.001$. Error bars represent one standard deviation.

Figure 2. Metabolomic analysis of *dLdh* mutants. Data from GC-MS metabolomic analysis (Supplemental Table 3) comparing *dLdh^{prec}* controls and *dLdh$^{16/17}$* mutants were analyzed using Metaboanalyst. (A) A volcano plot highlighting metabolites that exhibited a >1.5-fold change and a p-value of <0.01. *Note that changes in 2OG levels were not reproducible is subsequent experiments. (B) The relative abundance of metabolites that exhibited significant changes in all four GC-MS experiments ($P < 0.01$; see Supplemental Table 2). (C) The relative abundance of G3P was measured in *dLdh^{prec}* controls, *dLdh$^{16/17}$* mutants, and *p{dLdh}; dLdh$^{16/17}$* rescued animals during the L2 larval stage. (D) Lactate and G3P levels were measured in L2 larvae that ubiquitously expressed either a *UAS-GFP-RNAi* construct or a *UAS-dLdh-RNAi* construct under

the control of *da-GAL4*. Abbreviations as follow: lactate (Lac), 2-hydroxyglutarate (2HG), pyruvate (Pyr), glycerol-3-phosphate (G3P), 2-oxoglutarate (2OG), not significant (n.s.). n=6 samples collected from independent populations with 25 mid-L2 larvae per sample. *** $P < 0.001$.

Figure 3. GPDH1 controls NAD$^+$/NADH redox balance during larval development. (A) A schematic diagram illustrating how GPDH1 and dLDH redundantly influence NAD$^+$ levels. Abbreviations as follow: dihydroxyacetone phosphate (DHAP), glycerol-3-phosphate (G3P), pyruvate (Pyr), lactate (Lac). (B) GC-MS was used to measure relative G3P abundance in mid-L2 larvae for the following five genotypes: *Gpdh1$^{A10/+}$*, *Gpdh1$^{A10/B18}$*, *Gpdh1$^{A10/B18}$; da-GAL4*, *Gpdh$^{A10/B18}$; UAS-Gpdh1,* and *Gpdh1$^{A10/B18}$; da-GAL4 UAS-Gpdh1*. Data are represented as box plots, $n = 6$. ***$P < 0.001$. (C) The NAD$^+$/NADH ratio in mid-L2 larvae of the following genotypes: *dLdh^{prec}*, *dLdh$^{16/17}$*, *Gpdh1$^{A10/+}$*, and *Gpdh1$^{A10/B18}$*. (D) mid-L2 larvae were fed D-glucose-$^{13}C_6$ for two hours and the rate of ^{13}C isotope incorporation into lactate (Lac) and G3P was determined based on m+3 isotopologue abundance. (E) ATP levels are significantly decreased in *Gpdh1$^{A10/B18}$* as compared with *Gpdh1$^{A10/+}$* controls. (F) The body mass of *Gpdh1$^{A10/B18}$* larvae is significantly lower than that of *Gpdh1$^{A10/+}$* controls 0-4 hours after the L2-L3 molt. In panels (B-F), n=6 samples per genotype. ***$P < 0.001$. For (C-F), error bars represent one standard deviation.

Figure 4. *Gpdh1; dLdh* double mutants exhibit severe growth phenotypes. (A) Representative images of larvae from synchronized populations of *w^{1118}*, *dLdh$^{16/17}$*, *Gpdh1$^{A10/B18}$*, or *Gpdh1$^{A10/B18}$; dLdh$^{16/17}$* double mutants. Note the severe developmental delay exhibited by double mutant larvae. (B) The body mass of *w^{1118}* and *Gpdh1$^{A10/B18}$; dLdh$^{16/17}$* double mutant larvae measured 72 hours

after egg-laying. (C) The viability of the four genotypes listed in (A) were measured during defined periods of larval development. (B,C) Error bars represent one standard deviation. n=6 samples per genotype. (D-H) Maximum projections of dorsal half of L2 larval brains stained for Dpn (green) and DAPI (blue) from (D) w^{1118} controls, (E) $dLdh^{16/17}$ mutants, (F) $Gpdh1^{A10/B18}$ mutants, (G) age-matched $Gpdh1^{A10/B18}$; $dLdh^{16/17}$ double mutants, and (H) size-matched $Gpdh1^{A10/B18}$; $dLdh^{16/17}$ double mutants. The scale bar in (D) applies to (E-H). Note that the (D'-H') display the Dpn channel alone in gray scale. ***$P < 0.001$.

Figure 5. The DNA replication rate is decreased in brains of *Gpdh1; dLdh* double mutants (A-D) Maximum projections of dorsal half of size-matched L2 larval brains stained for EdU (red) and DAPI (blue) from (A) w^{1118} controls, (B) $dLdh^{16/17}$ mutants, (C) $Gpdh1^{A10/B18}$ mutants, and (D) $Gpdh1^{A10/B18}$; $dLdh^{16/17}$ double mutants. The scale bar in (A) applies to (A-D). Panels (A'-D') display EdU staining alone in gray scale. (E) Histogram of the number of EdU positive cells per dorsal brain lobe per genotype. For all panels, p-value adjusted for multiple comparisons using the Bonferroni-Dunn method. * $P < 0.05$. **P<0.01, ***$P < 0.001$.

Figure 6. Amino acid and glucose metabolism are disrupted in *Gpdh1; dLdh* double mutants. (A) The NAD^+/NADH ratio was measured in w^{1118}, $dLdh^{16/17}$, $Gpdh1^{A10/B18}$, and $Gpdh1^{A10/B18}$; $dLdh^{16/17}$ mid-L2 larvae. Error bars represent one standard deviation. n=6 samples per genotype. (B) A heat-map summarizing changes in metabolite abundance in $dLdh^{16/17}$ mutants relative to $dLdh^{prec}$ controls, $Gpdh1^{A10/B18}$ mutants relative to $Gpdh1^{A10/+}$ controls, and $Gpdh1^{A10/B18}$; $dLdh^{16/17}$ double mutants relative to $Gpdh1^{A10/+}$; $dLdh^{16/+}$ controls. The abundance of select metabolites for either (C) $Gpdh1^{A10/B18}$ mutants relative to $Gpdh1^{A10/+}$ controls or (D) $Gpdh1^{A10/B18}$; $dLdh^{16/17}$

577 double mutants relative to *Gpdh1*$^{A10/+}$; *dLdh*$^{16/+}$ are represented as box plots. For all panels, p-
578 value adjusted for multiple comparisons using the Bonferroni-Dunn method. * $P < 0.05$.
579 **P<0.01, ***$P < 0.001$.

580 **LITERATURE CITED**

581

582 **Avi-Dor, Y. and Mager, J.** (1956). The effect of fluoropyruvate on the respiration of animal-
583 tissue preparations. *Biochem J* **63**, 613-618.
584 **Backhaus, B., Sulkowski, E. and Schlote, F.** (1984). A semi-synthetic, general-purpose
585 medium for Drosophila melanogaster. *Dros. Inf. Serv* **60**, 210-212.
586 **Bewley, G. C. and Lucchesi, J. C.** (1977). Origin of alpha-glycerophosphate dehydrogenase
587 isozymes in Drosophila melanogaster and their functional relationship in the alpha-
588 glycerophosphate cycle. *Biochem Genet* **15**, 235-251.
589 **Billiard, J., Dennison, J. B., Briand, J., Annan, R. S., Chai, D., Colon, M., Dodson, C. S.,**
590 **Gilbert, S. A., Greshock, J., Jing, J., et al.** (2013). Quinoline 3-sulfonamides inhibit
591 lactate dehydrogenase A and reverse aerobic glycolysis in cancer cells. *Cancer Metab*
592 **1**, 19.
593 **Boudreau, A., Purkey, H. E., Hitz, A., Robarge, K., Peterson, D., Labadie, S., Kwong, M.,**
594 **Hong, R., Gao, M., Del Nagro, C., et al.** (2016). Metabolic plasticity underpins innate
595 and acquired resistance to LDHA inhibition. *Nat Chem Biol* **12**, 779-786.
596 **Boxer, G. E. and Shonk, C. E.** (1960). Low levels of soluble DPN-linked alpha-
597 glycerophosphate dehydrogenase in tumors. *Cancer Res* **20**, 85-91.
598 **Bricker, D. K., Taylor, E. B., Schell, J. C., Orsak, T., Boutron, A., Chen, Y. C., Cox, J. E.,**
599 **Cardon, C. M., Van Vranken, J. G., Dephoure, N., et al.** (2012). A mitochondrial
600 pyruvate carrier required for pyruvate uptake in yeast, *Drosophila*, and humans.
601 *Science* **337**, 96-100.
602 **Bulusu, V., Prior, N., Snaebjornsson, M. T., Kuehne, A., Sonnen, K. F., Kress, J., Stein, F.,**
603 **Schultz, C., Sauer, U. and Aulehla, A.** (2017). Spatiotemporal Analysis of a
604 Glycolytic Activity Gradient Linked to Mouse Embryo Mesoderm Development. *Dev*
605 *Cell* **40**, 331-341 e334.
606 **Chong, J., Soufan, O., Li, C., Caraus, I., Li, S., Bourque, G., Wishart, D. S. and Xia, J.** (2018).
607 MetaboAnalyst 4.0: towards more transparent and integrative metabolomics
608 analysis. *Nucleic Acids Res* **46**, W486-W494.
609 **Cooper, E. H., Barkhan, P. and Hale, A. J.** (1963). Observations on the proliferation of
610 human leucocytes cultured with phytohaemagglutinin. *Br J Haematol* **9**, 101-111.
611 **Cox, J. E., Thummel, C. S. and Tennessen, J. M.** (2017). Metabolomic Studies in *Drosophila*.
612 *Genetics* **206**, 1169-1185.
613 **Daniele, S., Giacomelli, C., Zappelli, E., Granchi, C., Trincavelli, M. L., Minutolo, F. and**
614 **Martini, C.** (2015). Lactate dehydrogenase-A inhibition induces human
615 glioblastoma multiforme stem cell differentiation and death. *Sci Rep* **5**, 15556.
616 **Duncan, D. M., Kiefel, P. and Duncan, I.** (2017). Mutants for Drosophila Isocitrate
617 Dehydrogenase 3b Are Defective in Mitochondrial Function and Larval Cell Death.
618 *G3* **7**, 789-799.
619 **Fantin, V. R., St-Pierre, J. and Leder, P.** (2006). Attenuation of LDH-A expression uncovers
620 a link between glycolysis, mitochondrial physiology, and tumor maintenance. *Cancer*
621 *Cell* **9**, 425-434.

Flores, A., Schell, J., Krall, A. S., Jelinek, D., Miranda, M., Grigorian, M., Braas, D., White, A. C., Zhou, J. L., Graham, N. A., et al. (2017). Lactate dehydrogenase activity drives hair follicle stem cell activation. *Nat Cell Biol* **19**, 1017-1026.

Goldberg, E. B. and Colowick, S. P. (1965). The Role of Glycolysis in the Growth of Tumor Cells. 3. Lactic Dehydrogenase as the Site of Action of Oxamate on the Growth of Cultured Cells. *J Biol Chem* **240**, 2786-2790.

Goldberg, E. B., Nitowsky, H. M. and Colowick, S. P. (1965). The Role of Glycolysis in the Growth of Tumor Cells. Iv. The Basis of Glucose Toxicity in Oxamate-Treated, Cultured Cells. *J Biol Chem* **240**, 2791-2796.

Gratz, S. J., Cummings, A. M., Nguyen, J. N., Hamm, D. C., Donohue, L. K., Harrison, M. M., Wildonger, J. and O'Connor-Giles, K. M. (2013). Genome engineering of Drosophila with the CRISPR RNA-guided Cas9 nuclease. *Genetics* **194**, 1029-1035.

Graveley, B. R., Brooks, A. N., Carlson, J. W., Duff, M. O., Landolin, J. M., Yang, L., Artieri, C. G., van Baren, M. J., Boley, N., Booth, B. W., et al. (2011). The developmental transcriptome of Drosophila melanogaster. *Nature* **471**, 473-479.

Hoekstra, L. A. and Montooth, K. L. (2013). Inducing extra copies of the Hsp70 gene in Drosophila melanogaster increases energetic demand. *BMC Evol Biol* **13**, 68.

Hoekstra, L. A., Siddiq, M. A. and Montooth, K. L. (2013). Pleiotropic effects of a mitochondrial-nuclear incompatibility depend upon the accelerating effect of temperature in Drosophila. *Genetics* **195**, 1129-1139.

Kanno, T., Sudo, K., Maekawa, M., Nishimura, Y., Ukita, M. and Fukutake, K. (1988). Lactate dehydrogenase M-subunit deficiency: a new type of hereditary exertional myopathy. *Clin Chim Acta* **173**, 89-98.

Kanno, T., Sudo, K., Takeuchi, I., Kanda, S., Honda, N., Nishimura, Y. and Oyama, K. (1980). Hereditary deficiency of lactate dehydrogenase M-subunit. *Clin Chim Acta* **108**, 267-276.

Li, H., Chawla, G., Hurlburt, A. J., Sterrett, M. C., Zaslaver, O., Cox, J., Karty, J. A., Rosebrock, A. P., Caudy, A. A. and Tennessen, J. M. (2017). *Drosophila* larvae synthesize the putative oncometabolite L-2-hydroxyglutarate during normal developmental growth. *Proc Natl Acad Sci U S A* **114**, 1353-1358.

Li, H. and Tennessen, J. M. (2017). Methods for studying the metabolic basis of Drosophila development. *Wiley Interdiscip Rev Dev Biol* **6**.

---- (2018). Preparation of Drosophila Larval Samples for Gas Chromatography-Mass Spectrometry (GC-MS)-based Metabolomics. *J Vis Exp*.

Li, Y., Padmanabha, D., Gentile, L. B., Dumur, C. I., Beckstead, R. B. and Baker, K. D. (2013). HIF- and non-HIF-regulated hypoxic responses require the estrogen-related receptor in Drosophila melanogaster. *PLoS Genet* **9**, e1003230.

Luhur, A., Buddika, K., Ariyapala, I. S., Chen, S. and Sokol, N. S. (2017). Opposing Post-transcriptional Control of InR by FMRP and LIN-28 Adjusts Stem Cell-Based Tissue Growth. *Cell Rep* **21**, 2671-2677.

Luhur, A., Chawla, G., Wu, Y. C., Li, J. and Sokol, N. S. (2014). Drosha-independent DGCR8/Pasha pathway regulates neuronal morphogenesis. *Proc Natl Acad Sci U S A* **111**, 1421-1426.

MacNeil, L. T., Watson, E., Arda, H. E., Zhu, L. J. and Walhout, A. J. (2013). Diet-induced developmental acceleration independent of TOR and insulin in C. elegans. *Cell* **153**, 240-252.

668 **Maekawa, M., Sudo, K., Kanno, T. and Li, S. S.** (1990). Molecular characterization of
669 genetic mutation in human lactate dehydrogenase-A (M) deficiency. *Biochem*
670 *Biophys Res Commun* **168**, 677-682.
671 **Mandal, S., Guptan, P., Owusu-Ansah, E. and Banerjee, U.** (2005). Mitochondrial
672 regulation of cell cycle progression during development as revealed by the tenured
673 mutation in Drosophila. *Dev Cell* **9**, 843-854.
674 **Matoo, O. B., Julick, C. R. and Montooth, K. L.** (2018). Genetic variation for ontogenetic
675 shifts in metabolism underlies physiological homeostasis in Drosophila. *bioRxiv*
676 **456269**.
677 **Mccabe, C. T. and Bursell, E.** (1975). Interrelationships between Amino-Acid and Lipid-
678 Metabolism in Tsetse-Fly, Glossina-Morsitans. *Insect Biochem* **5**, 781-789.
679 **Meiklejohn, C. D., Holmbeck, M. A., Siddiq, M. A., Abt, D. N., Rand, D. M. and Montooth,**
680 **K. L.** (2013). An Incompatibility between a mitochondrial tRNA and its nuclear-
681 encoded tRNA synthetase compromises development and fitness in Drosophila.
682 *PLoS Genet* **9**, e1003238.
683 **Miyajima, H., Takahashi, Y. and Kaneko, E.** (1995). Characterization of the glycolysis in
684 lactate dehydrogenase-A deficiency. *Muscle Nerve* **18**, 874-878.
685 **Miyazawa, H. and Aulehla, A.** (2018). Revisiting the role of metabolism during
686 development. *Development* **145**.
687 **O'Brien, S. J. and MacIntyre, R. J.** (1972). The -glycerophosphate cycle in Drosophila
688 melanogaster. I. Biochemical and developmental aspects. *Biochem Genet* **7**, 141-161.
689 **Oginuma, M., Moncuquet, P., Xiong, F., Karoly, E., Chal, J., Guevorkian, K. and**
690 **Pourquie, O.** (2017). A Gradient of Glycolytic Activity Coordinates FGF and Wnt
691 Signaling during Elongation of the Body Axis in Amniote Embryos. *Dev Cell* **40**, 342-
692 353 e310.
693 **Oliveira, M. T. and Kaguni, L. S.** (2011). Reduced stimulation of recombinant DNA
694 polymerase gamma and mitochondrial DNA (mtDNA) helicase by variants of
695 mitochondrial single-stranded DNA-binding protein (mtSSB) correlates with defects
696 in mtDNA replication in animal cells. *J Biol Chem* **286**, 40649-40658.
697 **Papaconstantinou, J. and Colowick, S. P.** (1961). The role of glycolysis in the growth of
698 tumor cells. I. Effects of oxamic acid on the metabolism of Ehrlich ascites tumor cells
699 in vitro. *J Biol Chem* **236**, 278-284.
700 **Pearce, E. L., Poffenberger, M. C., Chang, C. H. and Jones, R. G.** (2013). Fueling immunity:
701 insights into metabolism and lymphocyte function. *Science* **342**, 1242454.
702 **Qing, G., Skuli, N., Mayes, P. A., Pawel, B., Martinez, D., Maris, J. M. and Simon, M. C.**
703 (2010). Combinatorial regulation of neuroblastoma tumor progression by N-Myc
704 and hypoxia inducible factor HIF-1alpha. *Cancer Res* **70**, 10351-10361.
705 **Rechsteiner, M. C.** (1970). Drosophila lactate dehydrogenase and alpha-glycerolphosphate
706 dehydrogenase: distribution and change in activity during development. *J Insect*
707 *Physiol* **16**, 1179-1192.
708 **Schell, J. C., Wisidagama, D. R., Bensard, C., Zhao, H., Wei, P., Tanner, J., Flores, A.,**
709 **Mohlman, J., Sorensen, L. K., Earl, C. S., et al.** (2017). Control of intestinal stem cell
710 function and proliferation by mitochondrial pyruvate metabolism. *Nat Cell Biol* **19**,
711 1027-1036.

Sebo, Z. L., Lee, H. B., Peng, Y. and Guo, Y. (2014). A simplified and efficient germline-specific CRISPR/Cas9 system for Drosophila genomic engineering. *Fly (Austin)* **8**, 52-57.

Team, R. C. (2017). R: A language and environment for statistical computing. R Foundation for Statistical Computing.

Tennessen, J. M., Baker, K. D., Lam, G., Evans, J. and Thummel, C. S. (2011). The Drosophila estrogen-related receptor directs a metabolic switch that supports developmental growth. *Cell Metab* **13**, 139-148.

Tennessen, J. M., Barry, W. E., Cox, J. and Thummel, C. S. (2014a). Methods for studying metabolism in *Drosophila*. *Methods* **68**, 105-115.

Tennessen, J. M., Bertagnolli, N. M., Evans, J., Sieber, M. H., Cox, J. and Thummel, C. S. (2014b). Coordinated metabolic transitions during Drosophila embryogenesis and the onset of aerobic glycolysis. *G3* **4**, 839-850.

Tixier, V., Bataille, L., Etard, C., Jagla, T., Weger, M., Daponte, J. P., Strahle, U., Dickmeis, T. and Jagla, K. (2013). Glycolysis supports embryonic muscle growth by promoting myoblast fusion. *Proc Natl Acad Sci U S A* **110**, 18982-18987.

Vander Heiden, M. G., Cantley, L. C. and Thompson, C. B. (2009). Understanding the Warburg effect: the metabolic requirements of cell proliferation. *Science* **324**, 1029-1033.

Wang, L., Lam, G. and Thummel, C. S. (2010). *Med24* and *Mdh2* are required for *Drosophila* larval salivary gland cell death. *Dev Dyn* **239**, 954-964.

Wang, T., Marquardt, C. and Foker, J. (1976). Aerobic glycolysis during lymphocyte proliferation. *Nature* **261**, 702-705.

Warburg, O. (1956). On the origin of cancer cells. *Science* **123**, 309-314.

Warton, D. I., Wright, I. J., Falster, D. S. and Westoby, M. (2006). Bivariate line-fitting methods for allometry. *Biol Rev Camb Philos Soc* **81**, 259-291.

Watson, E., MacNeil, L. T., Ritter, A. D., Yilmaz, L. S., Rosebrock, A. P., Caudy, A. A. and Walhout, A. J. (2014). Interspecies systems biology uncovers metabolites affecting C. elegans gene expression and life history traits. *Cell* **156**, 759-770.

Watson, E., Olin-Sandoval, V., Hoy, M. J., Li, C. H., Louisse, T., Yao, V., Mori, A., Holdorf, A. D., Troyanskaya, O. G., Ralser, M., et al. (2016). Metabolic network rewiring of propionate flux compensates vitamin B12 deficiency in C. elegans. *Elife* **5**.

Xie, H., Hanai, J., Ren, J. G., Kats, L., Burgess, K., Bhargava, P., Signoretti, S., Billiard, J., Duffy, K. J., Grant, A., et al. (2014). Targeting lactate dehydrogenase--a inhibits tumorigenesis and tumor progression in mouse models of lung cancer and impacts tumor-initiating cells. *Cell Metab* **19**, 795-809.

Yoshikuni, K., Tagami, H., Yamada, M., Sudo, K. and Kanno, T. (1986). Erythematosquamous skin lesions in hereditary lactate dehydrogenase M-subunit deficiency. *Arch Dermatol* **122**, 1420-1424.

Zdralevic, M., Brand, A., Di Ianni, L., Dettmer, K., Reinders, J., Singer, K., Peter, K., Schnell, A., Bruss, C., Decking, S. M., et al. (2018). Double genetic disruption of lactate dehydrogenase A and B is required to ablate the 'Warburg effect' restricting tumor growth to oxidative metabolism. *J Biol Chem*.

Zebe, E. C. and McShan, W. H. (1957). Lactic and alpha-glycerophosphate dehydrogenases in insects. *J Gen Physiol* **40**, 779-790.

758

759 **Supplemental Figure Legends**

760

761 **Supplemental Figure 1. Mitochondrial abundance is unaffected by *dLdh* mutations.** (A) The
762 relative abundance of mitochondrial DNA is similar in $dLdh^{prec}$ controls and $dLdh^{16/17}$ mutants.
763 Ratio is based on the abundance of *mt::CoI* copy number relative to *Rpl32* copy number. Error
764 bars represent standard deviation.

765

766 **Supplemental Figure 2. Generation of *Gpdh1* mutants.** (A) A schematic diagram illustrating
767 the *Gpdh1* locus, sequences targeted by guide RNA constructs, and sequence deleted by the
768 $Gpdh1^{A10}$ and $Gpdh1^{B18}$ mutations. Deleted bases are highlighted in red. (B) A schematic diagram
769 illustrating the location of the $Gpdh1^{A10}$ and $Gpdh1^{B18}$ mutations within the GPDH1 protein. (C)
770 $Gpdh1^{A10/+}$, and $Gpdh1^{A10/B18}$ mutants were analyzed for larval viability. Bars represent the percent
771 of animals that survived from the previous developmental stage until the stage noted on the x-axis.
772 Error bars represent standard deviation. n>100 larvae per timepoint.

773

774 **Supplemental Figure 3. The intestine of $Gpdh^{A10/B18}$; $dLdh^{16/17}$ double mutant larvae exhibit**
775 **growth defects and contain smaller cells.** (A-E) L2 larval posterior midguts (PMGs) stained for
776 DAPI (gray) from (A) w^{1118} controls, (B) $Gpdh1^{A10/B18}$ mutants, (C) $dLdh^{16/17}$ mutants, (D) age-
777 matched $Gpdh1^{A10/B18}$; $dLdh^{16/17}$ double mutants, and (E) size-matched $Gpdh1^{A10/B18}$; $dLdh^{16/17}$
778 double mutants. (A'-E') Magnified images of the outlined regions in A-E. The scale bar in (E) and
779 (E') apply to (A-E) and (A'-E'), respectively. (F) Histogram of nuclei size. **** $P < 0.0001$.

780

Supplemental Figure 4. *Gpdh1; dLdh* double mutants exhibit significant changes in purine catabolism and ATP production. GC-MS was used to measure the relative abundance of xanthine and urate in either (A) $Gpdh1^{A10/B18}$ mutants relative to $Gpdh1^{A10/+}$ controls or (B) $Gpdh1^{A10/B18}$; $dLdh^{16/17}$ double mutants relative to $Gpdh1^{A10/+}$; $dLdh^{16/+}$. (C) ATP levels are significantly decreased in $Gpdh1^{A10/B18}$; $dLdh^{16/17}$ double mutants relative to $Gpdh1^{A10/+}$; $dLdh^{16/+}$. ***$P < 0.001$.

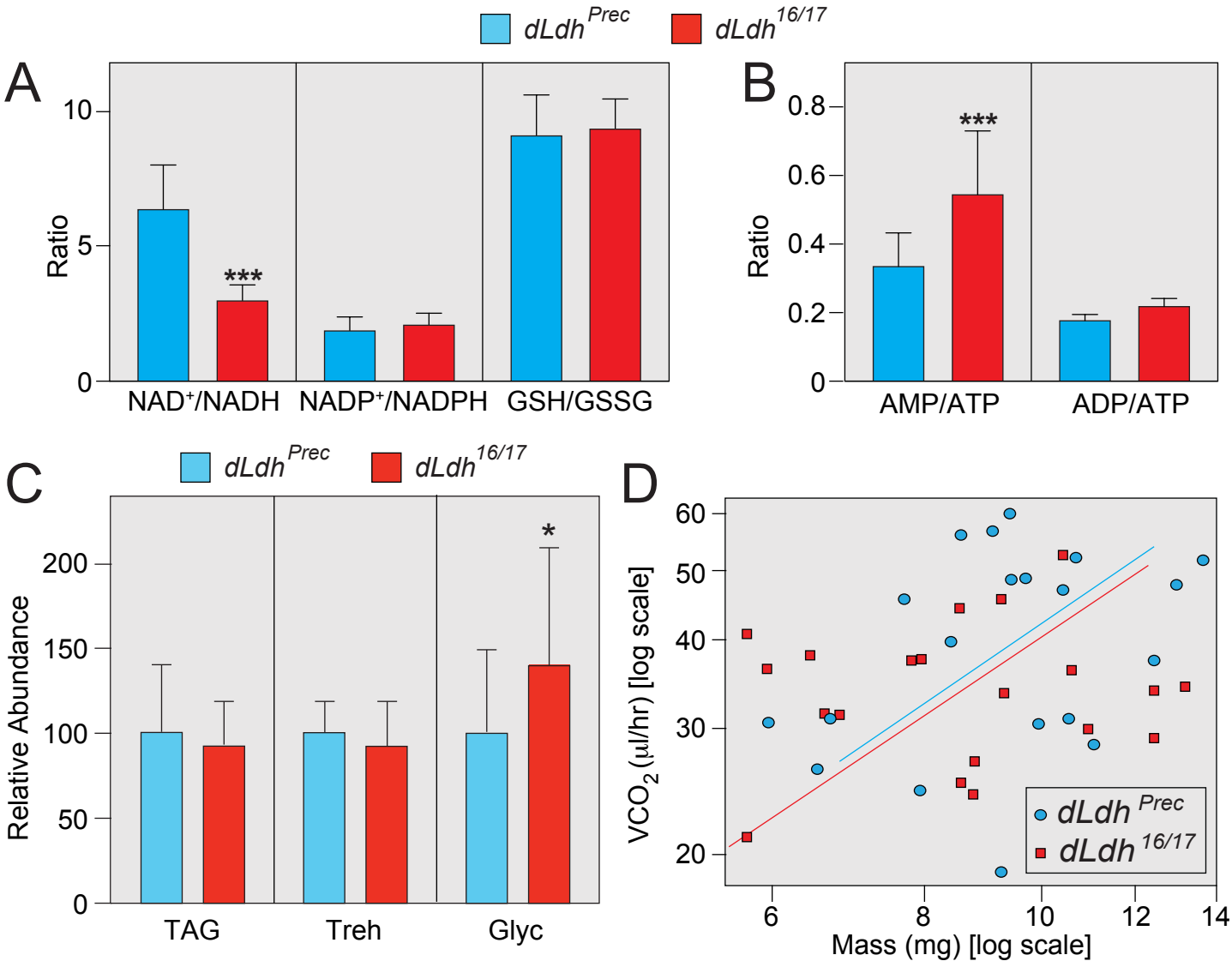

Figure 1. dLDH maintains the NAD⁺/NADH redox balance during larval development. Targeted LC-MS/MS analysis was used to measure metabolites associated with redox balance in *dLdh*^{prec} controls and *dLdh*$^{16/17}$ mutants. The ratio of (A-B) NAD⁺/NADH, NADP⁺/NADPH, GSH/GSSG, AMP/ATP and ADP/ATP were determined in control and mutant larvae. n=8 samples collected from independent populations with 100 mid-L2 larvae per sample. (C) *dLdh*^{prec} controls and *dLdh*$^{16/17}$ mutants were collected as mid-L2 larvae and the concentration of triglycerides (TAG), trehalose (Treh), and glycogen (Glyc) were measured in whole animal homogenates. All data were normalized to soluble protein. For all assays, n>10 samples collected from independent populations with 25 mid-L2 larvae per sample. (D) The rate of CO_2 production was measured *dLdh*$^{16/17}$ mutants and precise excision controls. For (A-C), * $P < 0.05$. *** $P < 0.001$. Error bars represent one standard deviation.

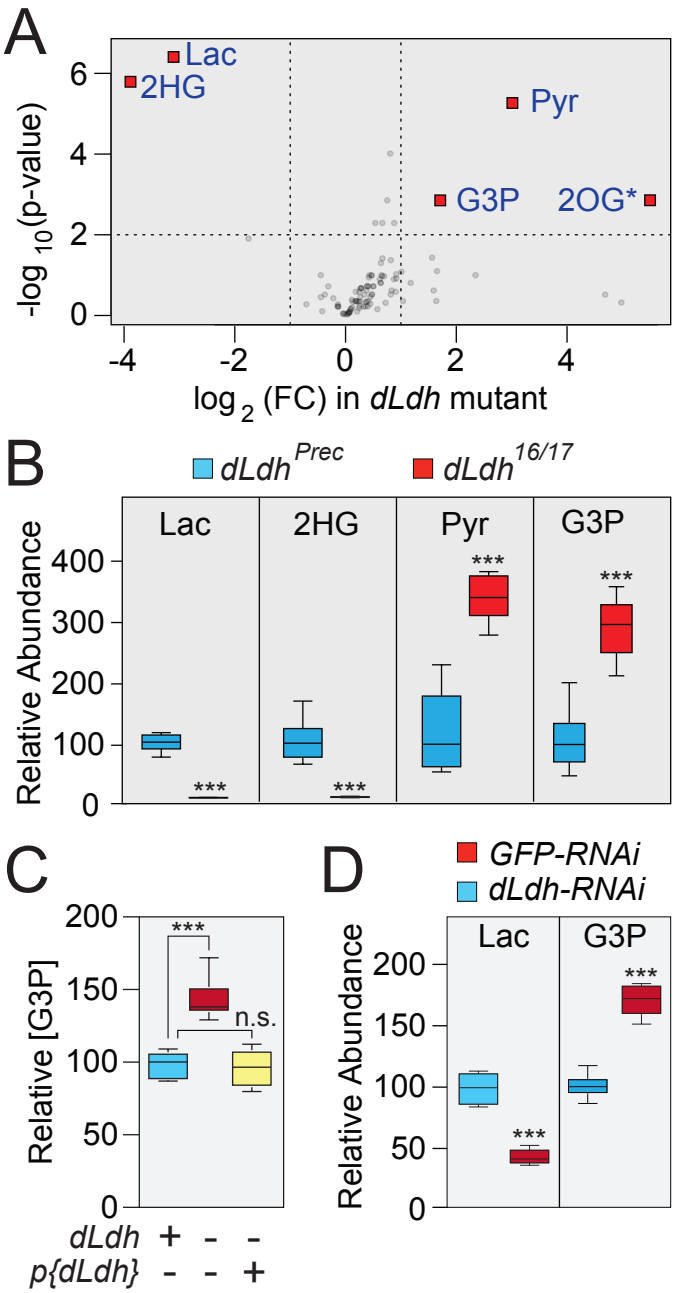

Figure 2. Metabolomic analysis of *dLdh* mutants. Data from GC-MS metabolomic analysis (Supplemental Table 3) comparing $dLdh^{prec}$ controls and $dLdh^{16/17}$ mutants were analyzed using Metaboanalyst. (A) A volcano plot highlighting metabolites that exhibited a >1.5-fold change and a p-value of <0.01. *Note that changes in 2OG levels were not reproducible is subsequent experiments. (B) The relative abundance of metabolites that exhibited significant changes in all four GC-MS experiments ($P < 0.01$; see Supplemental Table 2). (C) The relative abundance of G3P was measured in $dLdh^{prec}$ controls, $dLdh^{16/17}$ mutants, and *p{dLdh}; $dLdh^{16/17}$* rescued animals during the L2 larval stage. (D) Lactate and G3P levels were measured in L2 larvae that ubiquitously expressed either a *UAS-GFP-RNAi* construct or a *UAS-dLdh-RNAi* construct under the control of *da-GAL4*. Abbreviations as follow: lactate (Lac), 2-hydroxyglutarate (2HG), pyruvate (Pyr), glycerol-3-phosphate (G3P), 2-oxoglutarate (2OG), not significant (n.s.). n=6 samples collected from independent populations with 25 mid-L2 larvae per sample. *** $P < 0.001$.

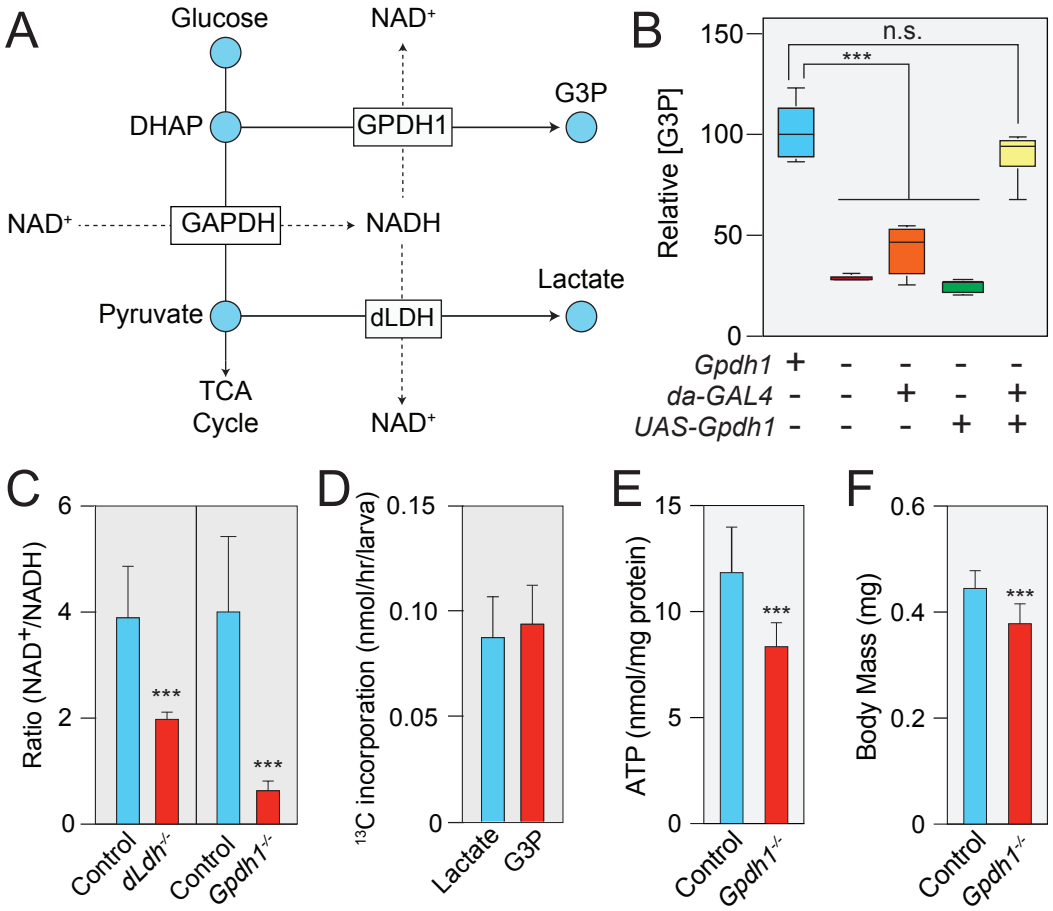

Figure 3. GPDH1 controls NAD$^+$/NADH redox balance during larval development. (A) A schematic diagram illustrating how GPDH1 and dLDH redundantly influence NAD$^+$ levels. Abbreviations as follow: dihydroxyacetone phosphate (DHAP), glycerol-3-phosphate (G3P), pyruvate (Pyr), lactate (Lac). (B) GC-MS was used to measure relative G3P abundance in mid-L2 larvae for the following five genotypes: *Gpdh1$^{A10/+}$*, *Gpdh1$^{A10/B18}$*, *Gpdh1$^{A10/B18}$; da-GAL4*, *Gpdh$^{A10/B18}$; UAS-Gpdh1,* and *Gpdh1$^{A10/B18}$; da-GAL4 UAS-Gpdh1*. Data are represented as box plots, n = 6. ***P < 0.001. (C) The NAD$^+$/NADH ratio in mid-L2 larvae of the following genotypes: *dLdh^{prec}*, *dLdh$^{16/17}$*, *Gpdh1$^{A10/+}$*, and *Gpdh1$^{A10/B18}$*. (D) mid-L2 larvae were fed D-glucose-$^{13}C_6$ for two hours and the rate of ^{13}C isotope incorporation into lactate (Lac) and G3P was determined based on m+3 isotopologue abundance. (E) ATP levels are significantly decreased in *Gpdh1$^{A10/B18}$* as compared with *Gpdh1$^{A10/+}$* controls. (F) The body mass of *Gpdh1$^{A10/B18}$* larvae is significantly lower than that of *Gpdh1$^{A10/+}$* controls 0-4 hours after the L2-L3 molt. In panels (B-F), n=6 samples per genotype. ***P < 0.001. For (C-F), error bars represent one standard deviation.

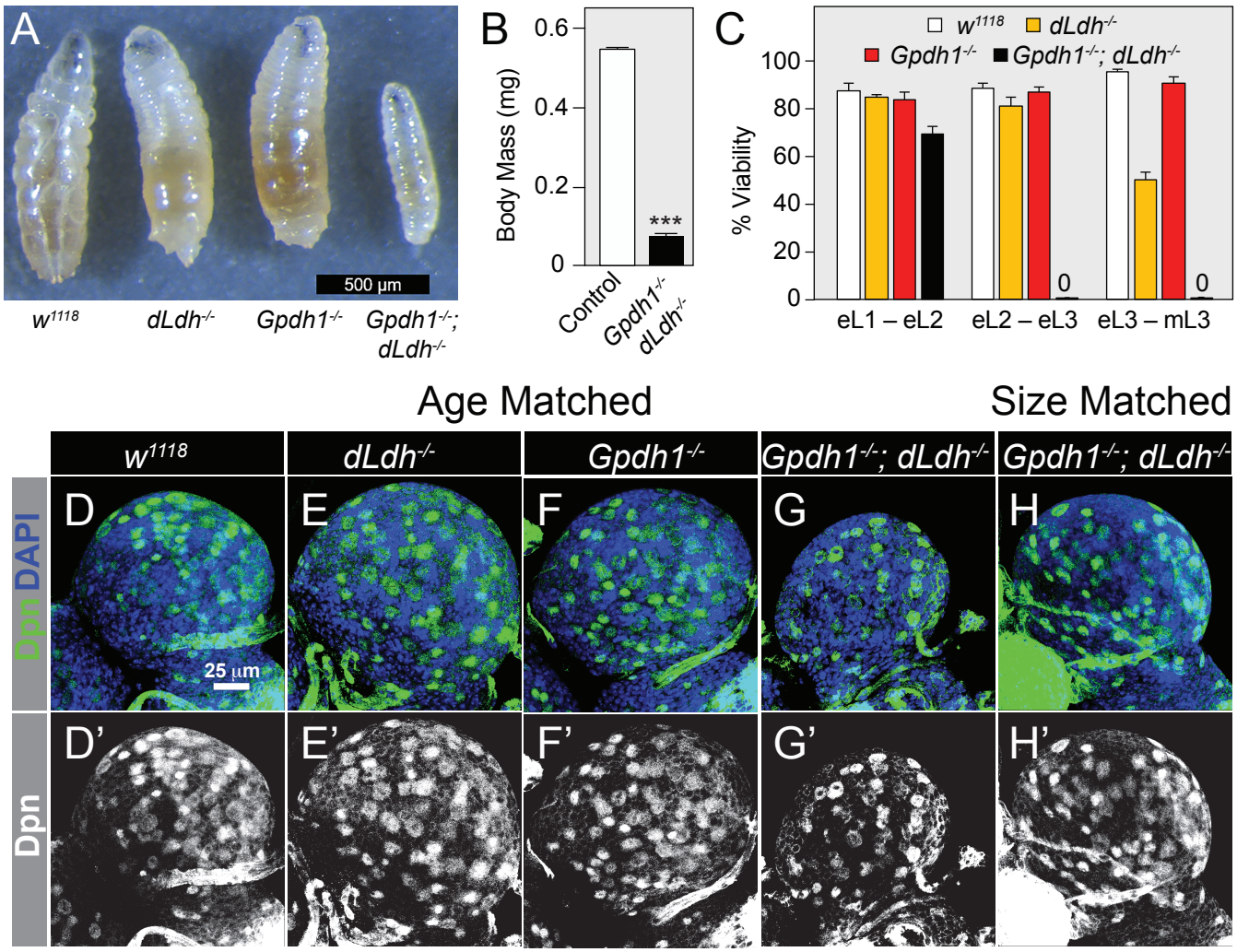

Figure 4. *Gpdh1; dLdh* double mutants exhibit severe growth phenotypes. (A) Representative images of larvae from synchronized populations of w^{1118}, $dLdh^{16/17}$, $Gpdh1^{A10/B18}$, or $Gpdh1^{A10/B18}$; $dLdh^{16/17}$ double mutants. Note the severe developmental delay exhibited by double mutant larvae. (B) The body mass of w^{1118} and $Gpdh1^{A10/B18}$; $dLdh^{16/17}$ double mutant larvae measured 72 hours after egg-laying. (C) The viability of the four genotypes listed in (A) were measured during defined periods of larval development. (B,C) Error bars represent one standard deviation. n=6 samples per genotype. (D-H) Maximum projections of dorsal half of L2 larval brains stained for Dpn (green) and DAPI (blue) from (D) w^{1118} controls, (E) $dLdh^{16/17}$ mutants, (F) $Gpdh1^{A10/B18}$ mutants, (G) age-matched $Gpdh1^{A10/B18}$; $dLdh^{16/17}$ double mutants, and (H) size-matched $Gpdh1^{A10/B18}$; $dLdh^{16/17}$ double mutants. The scale bar in (D) applies to (E-H). Note that the (D'-H') display the Dpn channel alone in gray scale. ***$P < 0.001$.

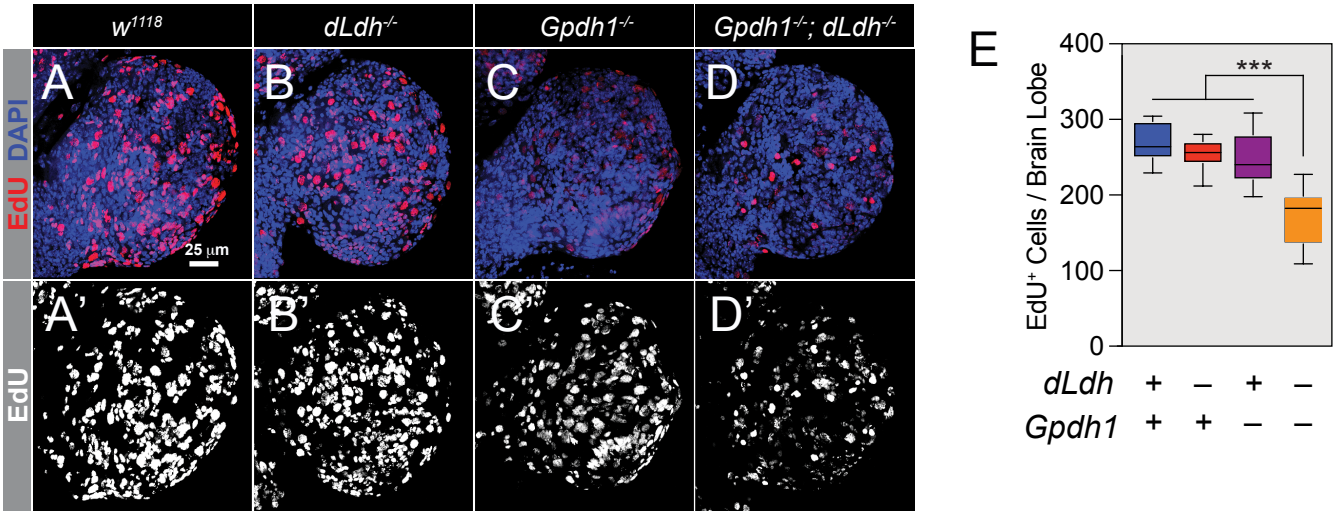

Figure 5. The DNA replication rate is decreased in brains of *Gpdh1; dLdh* double mutants (A-D) Maximum projections of dorsal half of size-matched L2 larval brains stained for EdU (red) and DAPI (blue) from (A) w^{1118} controls, (B) $dLdh^{16/17}$ mutants, (C) $Gpdh1^{A10/B18}$ mutants, and (D) $Gpdh1^{A10/B18}$; $dLdh^{16/17}$ double mutants. The scale bar in (A) applies to (A-D). Panels (A'-D') display EdU staining alone in gray scale. (E) Histogram of the number of EdU positive cells per dorsal brain lobe per genotype. For all panels, p-value adjusted for multiple comparisons using the Bonferroni-Dunn method. * $P < 0.05$. **P<0.01, ***$P < 0.001$.

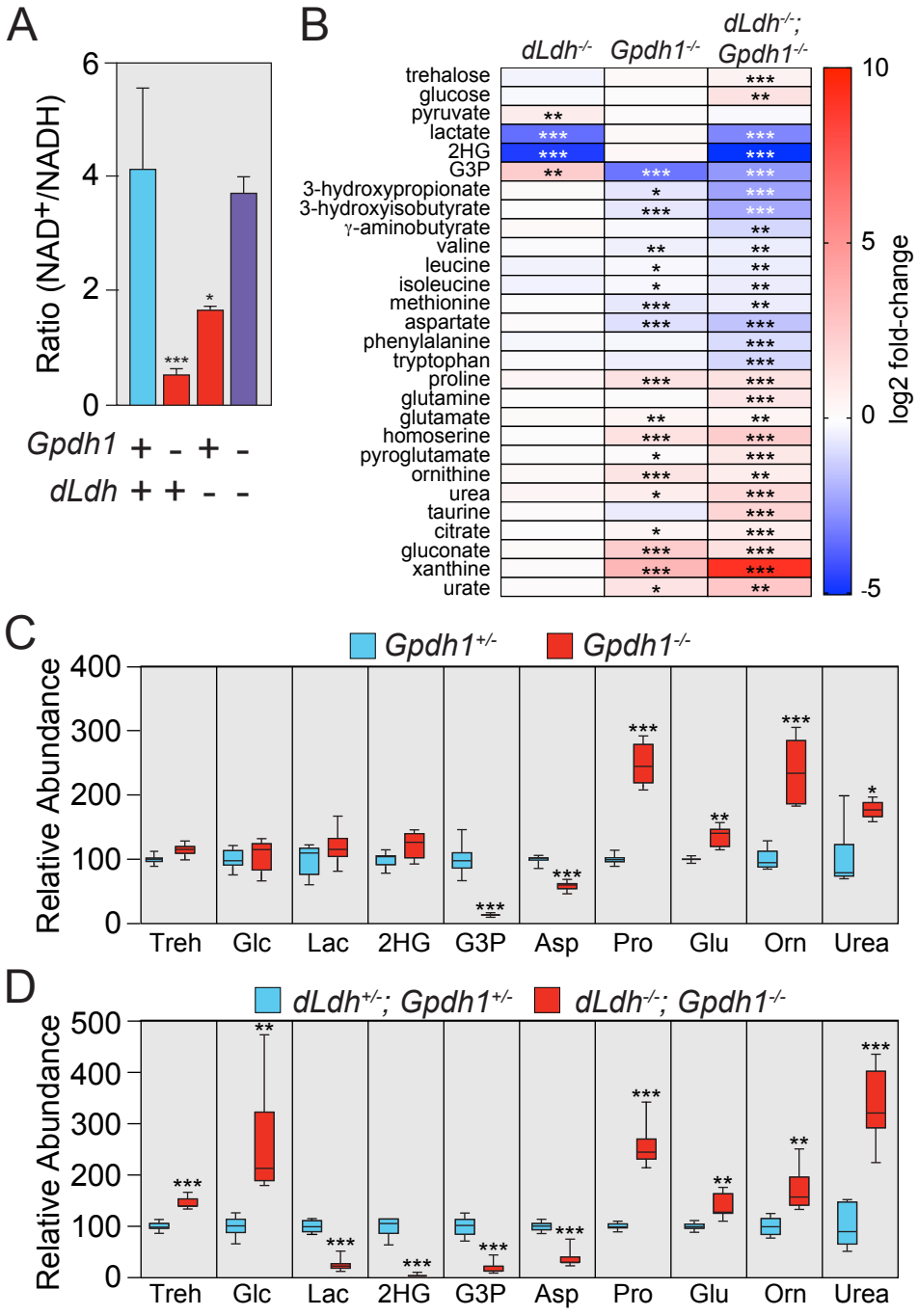

Figure 6. Amino acid and glucose metabolism are disrupted in *Gpdh1; dLdh* double mutants. (A) The NAD$^+$/NADH ratio was measured in w^{1118}, $dLdh^{16/17}$, $Gpdh1^{A10/B18}$, and $Gpdh1^{A10/B18}$; $dLdh^{16/17}$ mid-L2 larvae. Error bars represent one standard deviation. n=6 samples per genotype. (B) A heat-map summarizing changes in metabolite abundance in $dLdh^{16/17}$ mutants relative to $dLdh^{prec}$ controls, $Gpdh1^{A10/B18}$ mutants relative to $Gpdh1^{A10/+}$ controls, and $Gpdh1^{A10/B18}$; $dLdh^{16/17}$ double mutants relative to $Gpdh1^{A10/+}$; $dLdh^{16/+}$ controls. The abundance of select metabolites for either (C) $Gpdh1^{A10/B18}$ mutants relative to $Gpdh1^{A10/+}$ controls or (D) $Gpdh1^{A10/B18}$; $dLdh^{16/17}$ double mutants relative to $Gpdh1^{A10/+}$; $dLdh^{16/+}$ are represented as box plots. For all panels, p-value adjusted for multiple comparisons using the Bonferroni-Dunn method. * $P < 0.05$. **P<0.01, ***$P < 0.001$.

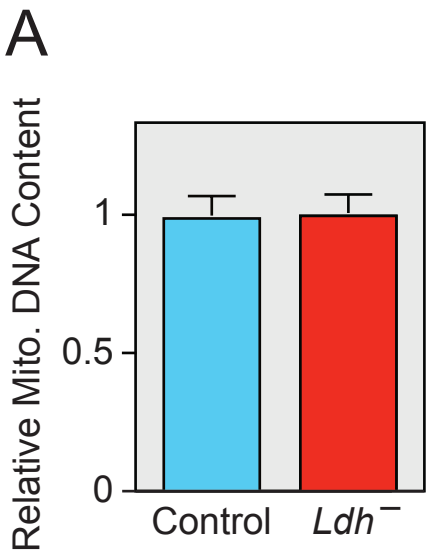

Supplemental Figure 1. Mitochondrial abundance is unaffected by *dLdh* mutations. (A) The relative abundance of mitochondrial DNA is similar in *dLdh*^{prec} controls and *dLdh*$^{16/17}$ mutants. Ratio is based on the abundance of *mt::CoI* copy number relative to *Rpl32* copy number. Error bars represent standard deviation.

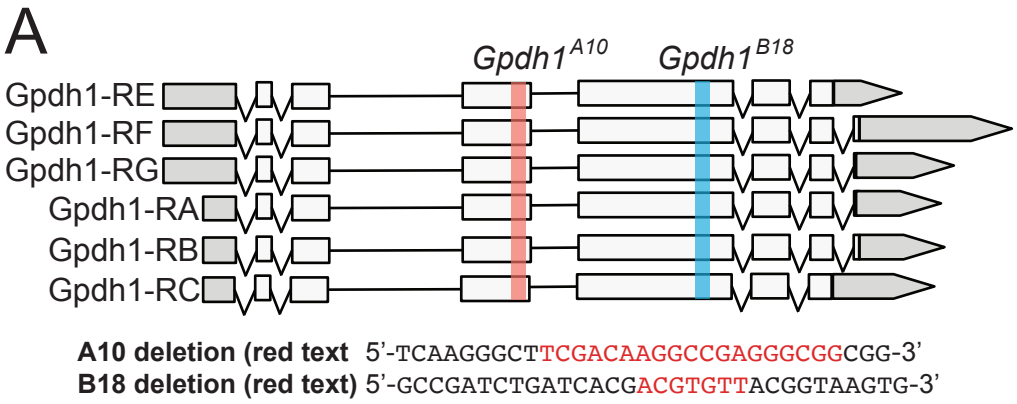

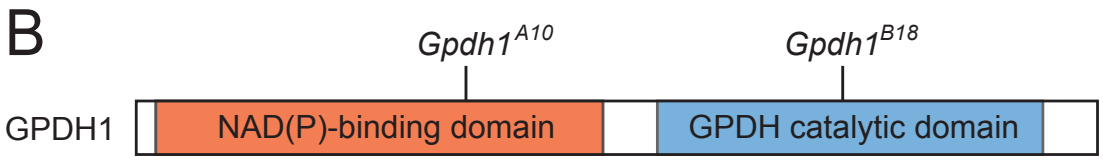

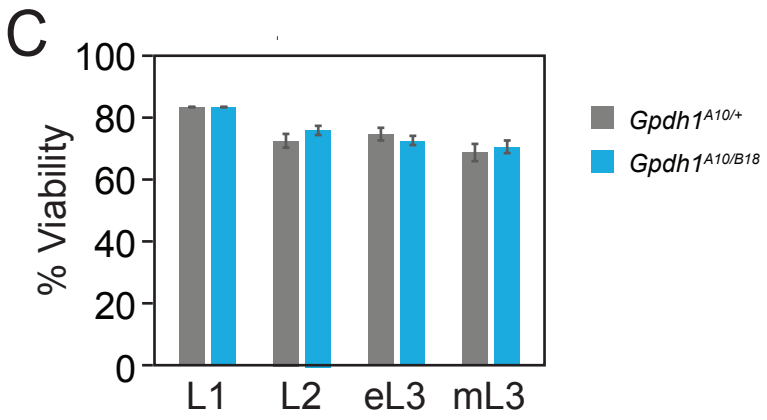

Supplemental Figure 2. Generation of *Gpdh1* mutants. (A) A schematic diagram illustrating the *Gpdh1* locus, sequences targeted by guide RNA constructs, and sequence deleted by the $Gpdh1^{A10}$ and $Gpdh1^{B18}$ mutations. Deleted bases are highlighted in red. (B) A schematic diagram illustrating the location of the $Gpdh1^{A10}$ and $Gpdh1^{B18}$ mutations within the GPDH1 protein. (C) $Gpdh1^{A10/+}$, and $Gpdh1^{A10/B18}$ mutants were analyzed for larval viability. Bars represent the percent of animals that survived from the previous developmental stage until the stage noted on the x-axis. Error bars represent standard deviation. n>100 larvae per timepoint.

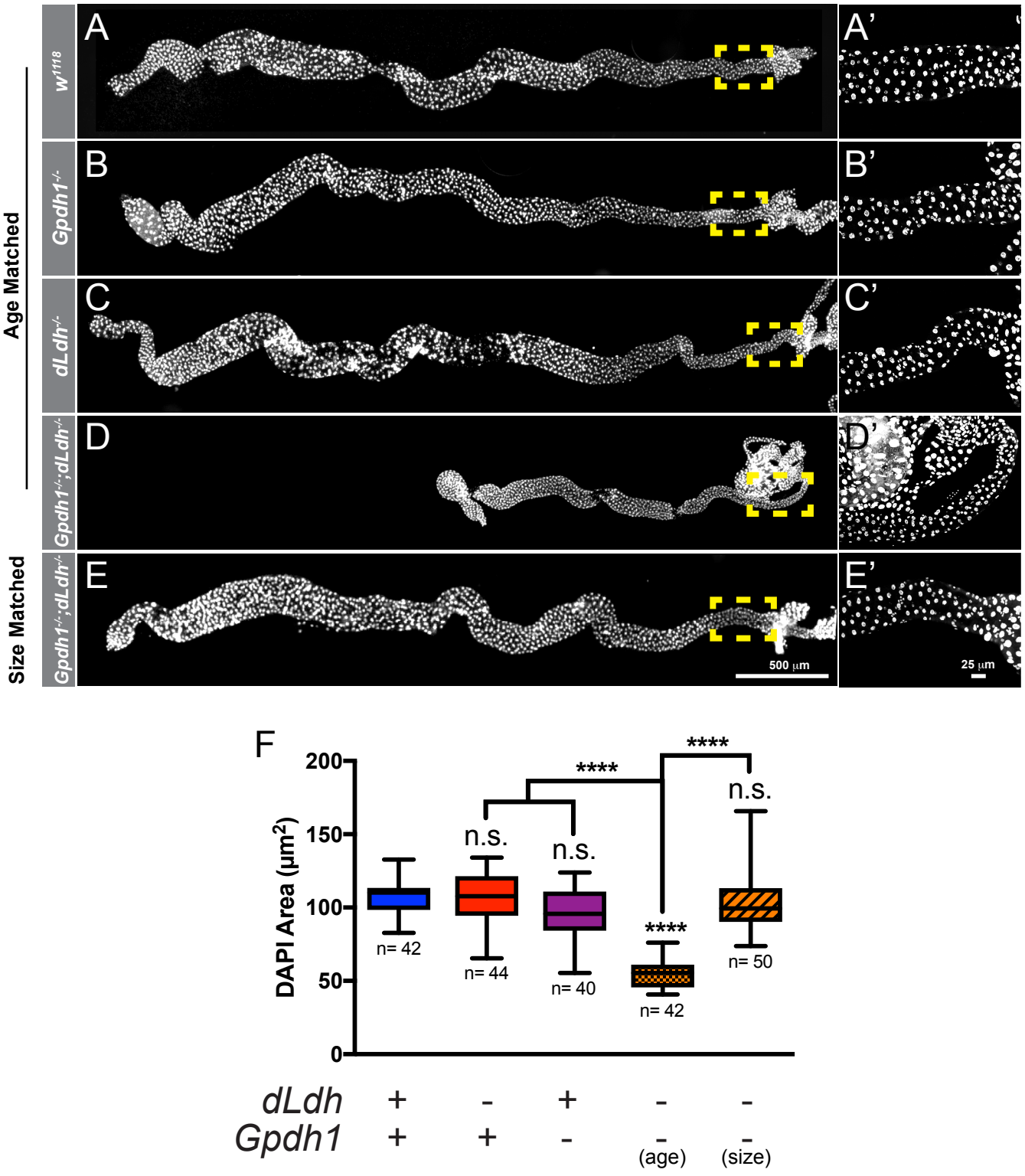

Supplemental Figure 3. The intestine of *Gpdh*$^{A10/B18}$; *dLdh*$^{16/17}$ double mutant larvae exhibit growth defects and contain smaller cells. (A-E) L2 larval posterior midguts (PMGs) stained for DAPI (gray) from (A) *w*^{1118} controls, (B) *Gpdh1*$^{A10/B18}$ mutants, (C) *dLdh*$^{16/17}$ mutants, (D) age-matched *Gpdh1*$^{A10/B18}$; *dLdh*$^{16/17}$ double mutants, and (E) size-matched *Gpdh1*$^{A10/B18}$; *dLdh*$^{16/17}$ double mutants. (A'-E') Magnified images of the outlined regions in A-E. The scale bar in (E) and (E') apply to (A-E) and (A'-E'), respectively. (F) Histogram of nuclei size. **** P < 0.0001.

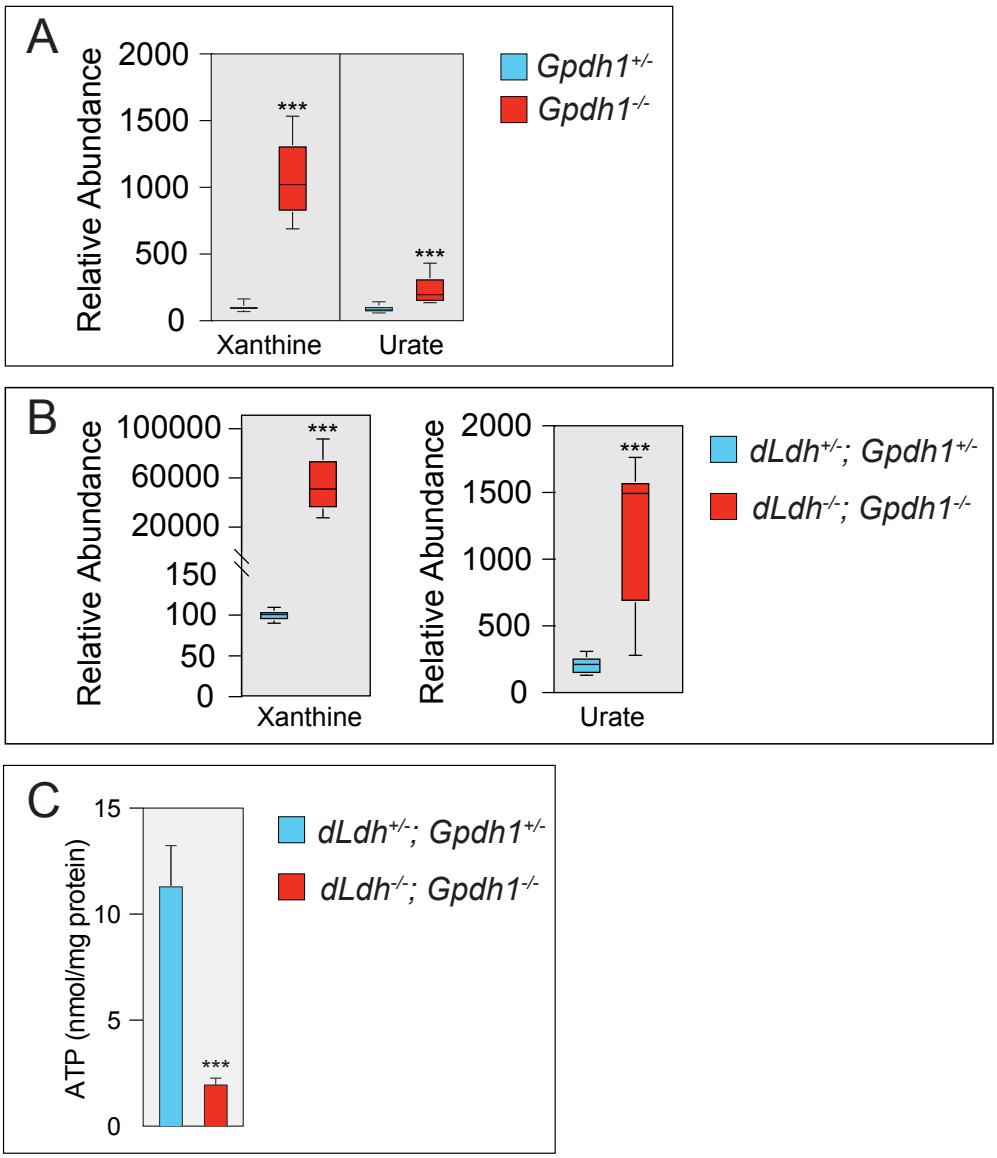

Supplemental Figure 4. *Gpdh1; dLdh* double mutants exhibit significant changes in purine catabolism and ATP production. GC-MS was used to measure the relative abundance of xanthine and urate in either (A) $Gpdh1^{A10/B18}$ mutants relative to $Gpdh1^{A10/+}$ controls or (B) $Gpdh1^{A10/B18}$; $dLdh^{16/17}$ double mutants relative to $Gpdh1^{A10/+}$; $dLdh^{16/+}$. (C) ATP levels are significantly decreased in $Gpdh1^{A10/B18}$; $dLdh^{16/17}$ double mutants relative to $Gpdh1^{A10/+}$; $dLdh^{16/+}$. ***$P < 0.001$.